Categorization of High-Wind Events and Their Contribution to the Seasonal Breakdown of Stratification on the Southern New England Shelf

Lukas Lobert[1,2], **Glen Gawarkiewicz**[1], **Albert Plueddemann**[1]

[1]Woods Hole Oceanographic Institution, Woods Hole, MA, USA
[2]Massachusetts Institute of Technology, Cambridge, MA, USA

Key Points:

- Destratification on the outer shelf occurs predominantly during high-wind events with downwelling-favorable wind forcing during early fall.
- Cyclones passing south of the shelf and large-scale high-pressure systems over East Canada are most impactful in removing stratification.
- Differences in the dominant mixing processes likely lead to opposite T/S-contributions to destratification for the impactful wind patterns.

Corresponding author: Lukas Lobert, `llobert@whoi.edu`

Abstract

High-wind events predominantly cause the rapid breakdown of seasonal stratification on the continental shelf. Although previous studies have shown how coastal stratification depends on local wind-forcing characteristics, the locally observed ocean forcing has not yet been linked to regional atmospheric weather patterns that determine the local wind characteristics. Establishing such a connection is a necessary first step towards examining how an altered atmospheric forcing due to climate change affects coastal ocean conditions. Here, we propose a categorization scheme for high-wind events that links atmospheric forcing patterns with changes in stratification. We apply the scheme to the Southern New England shelf utilizing observations from the Ocean Observatories Initiative Coastal Pioneer Array (2015-2022). Impactful wind forcing patterns occur predominantly during early fall, have strong downwelling-favorable winds, and are primarily of two types: i) Cyclonic storms that propagate south of the continental shelf causing anticyclonically rotating winds, and ii) persistent large-scale high-pressure systems over eastern Canada causing steady north-easterly winds. These patterns are associated with opposite temperature and salinity contributions to destratification, implying differences in the dominant processes driving ocean mixing. Cyclonic storms are associated with the strongest local wind energy input and drive mechanical mixing and surface cooling. In contrast, steady downwelling-favorable winds from high-pressure systems likely advect salty and less buoyant Slope Water onto the shelf. The high-wind event categorization scheme allows a transition from solely focusing on local wind forcing to considering realistic atmospheric weather patterns when investigating their impact on stratification in the coastal ocean.

Plain Language Summary

While coastal waters are strongly density-layered during the summer (called 'seasonal stratification'), high-wind events during the fall mix the water column and homogenize it. While it is known which local wind conditions tend to mix coastal waters the most, these conditions have not yet been linked to regional atmospheric weather patterns. Drawing such a connection is a necessary step towards understanding how atmospheric climate change may affect the coastal ocean. Here, we propose a categorization scheme to identify which atmospheric patterns have the strongest impact on coastal ocean stratification in the fall. The scheme is applied to the coastal ocean south of New England using seven years of mooring observations. Two weather categories are particularly impactful: Storms passing south of the coastal ocean and large-scale high-pressure systems over eastern Canada. Both categories occur mainly during early fall and bring north-easterly winds associated with the onshore movement of more dense open-ocean water which results in enhanced mixing. Differences in their ocean impact are likely caused by the difference in wind direction steadiness of the two categories. The categorization scheme allows a transition from solely investigating the ocean impacts from local wind forcing to incorporating more realistic atmospheric weather patterns.

1 Level 1 Head: Introduction

The annual cycle of stratification is the dominant mode of variability on the Southern New England continental shelf (abbreviated as SNES and shown in the inset of Fig. 1) on seasonal time scales (Beardsley et al., 1976). The onset and breakdown of stratification marks the transition between two distinct dynamical regimes on the continental shelf and is temporally aligned with blooms in primary production (Schofield et al., 2008) in one of the biologically most productive regions worldwide (O'Reilly & Zetlin, 1998). While the water column is homogenized during winter, surface heating in the spring heats up the surface layer while the interior stays considerably cooler. A seasonal pycnocline forms and reaches its maximum buoyancy gradient in late summer before strat-

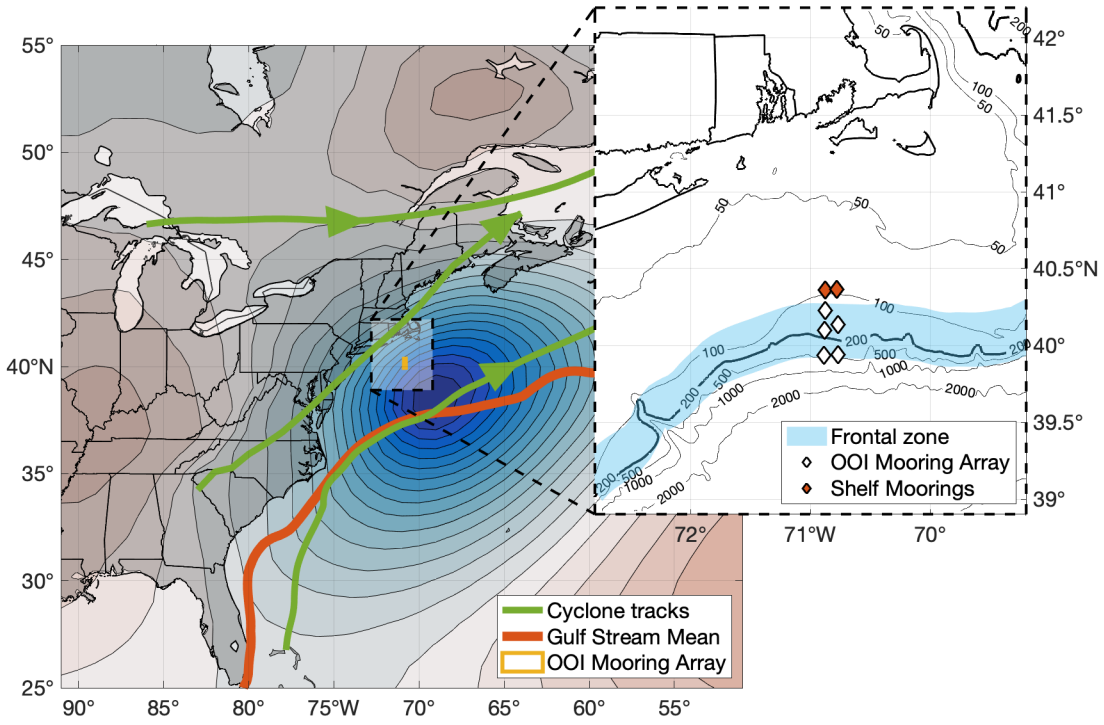

Figure 1. Map of Eastern North America and the Northwest Atlantic with a low-pressure system south of the Southern New England shelf (contours are sea level pressure). Shown are the two dominant cyclone tracks that pass north of the shelf and one cyclone track passing south, circulation features (shelfbreak frontal zone and mean Gulf Stream position), the Southern New England shelf bathymetry, and the location of the OOI Coastal Pioneer Array moorings. Mean storm tracks are derived from manually tracked cyclones during the fall seasons 2015-2021. The mean Gulf Stream position is approximated by the 0.25 cm isoline of the absolute dynamic topography climatological mean (generated using AVISO+ products (AVISO+, 2022)).

ification breaks down rapidly during fall (Linder & Gawarkiewicz, 1998). Lentz et al. (2003) observed that shelf destratification is clustered around storm events, suggesting that seasonal surface cooling plays a less crucial role than high-wind events.

Local wind forcing patterns in the region and their leading-order effects on shelf stratification are well understood. Northeasterly high-wind forcing during fall is associated with rapid destratification (Lentz et al., 2003), following a simple Ekman-forcing argument for the coastal ocean (Gill, 1982): Steady downwelling-favorable (easterly) winds are associated with destratification since they advect denser surface water from the Slope Sea onshore over more buoyant shelf water and can cause enhanced mixing at the shelfbreak due to frontal steepening (shelfbreak frontal zone is shown in Fig. 1). In contrast, upwelling-favorable winds are typically associated with restratification. Including such advection processes across the shelfbreak front is necessary to explain the rapidity of the stratification breakdown on the New Jersey shelf (Forsyth et al., 2018). As their model study was based significantly further inshore than observations used in this study, an even larger influence of frontal processes contributing to the observed variability can be expected on the outer shelf.

Even though the leading-order characteristics of wind-driven stratification changes are well understood, locally observed high-wind forcing on the continental shelf has not yet been linked to spatio-temporal atmospheric weather patterns. A more comprehensive view of wind-driven ocean forcing is vital to determine which atmospheric forcing patterns have the strongest impact on shelf stratification. Matching ocean impact with atmospheric patterns is a necessary first step towards elucidating how the seasonal cycle of stratification on the SNES responds to the changing nature of atmospheric forcing.

With climate change affecting wind forcing patterns, the timing of the rapid breakdown of stratification on the continental shelf during fall is likely subject to change. Atmospheric changes include a northward shift of Northern American storm tracks (Bengtsson et al. (2006) and Fig. 1) as well as a weaker and wavier polar jet stream due to Arctic Amplification (Francis & Vavrus, 2012). The boreal jet stream's waviness increased the most over North America and the North Atlantic, with the more drastic changes in fall and winter (Francis & Vavrus, 2015), i.e., the time period of interest for this study.

Here, we introduce a categorization scheme based on the spatio-temporal characteristics of high-wind events to identify which atmospheric patterns contribute most to the annual breakdown of stratification. The approach of categorizing high-wind forcing patterns to identify differences in the coastal ocean response has been proven successful for the Beaufort Sea continental shelfbreak (Foukal et al., 2019). Scalar metrics, encapsulating simplified wind forcing and ocean response variables, allow for easy comparison between events across multiple years of observations. While these simplifying metrics cannot capture the full dynamics of a high-wind forcing event, they allow focusing on the first-order forcing and impact characteristics to determine which events are most important for the seasonal destratification. By focusing not only on cyclones but on all types of weather systems associated with high-wind forcing, a more comprehensive understanding of the factors contributing the most to the seasonal breakdown of ocean stratification in the fall can be gained.

Section 2 introduces the data and methods used to identify high-wind events and their ocean impact on the SNES, followed by section 3 covering the observed interannual variability in destratifying the continental shelf during fall. The spatio-temporal high-wind event categorization scheme is described in section 4 before section 5 applies the scheme to distinguish between forcing and ocean impact characteristics. The manner in which the categorization scheme helps explain the variability of the seasonal impact, event timing, and mixing contributions are discussed in section 6.

2 Level 1 Head: Data and Methods

2.1 Level 2 Head: OOI Coastal Pioneer Array

Local atmospheric and subsurface information from the SNES has been recorded by the inshore moorings of the Ocean Observatories Initiative (OOI) Coastal Pioneer Array (abbreviated CP Array and mooring locations marked Fig. 1), a process-oriented shelfbreak observatory in operation between 2015-2022. The CP Array spans across the shelfbreak and is located close to the so-called '40/70 benchmark' at 40°N and 70°W, used by weather forecasters to estimate winter storm impacts for the US Northeast based on storm track positions relative to this point (Roller et al., 2016). The CP Array moorings feature surface buoys with meteorological sensors to determine bulk surface fluxes. Subsurface information is provided through wired profilers with Conductivity-Temperature-Depth (CTD) sensors in the central water column and fixed instrument packages within the surface and bottom boundary layers. This combination of assets makes the mooring array well-suited for quantifying high-wind surface forcing impacts on subsurface temperature, salinity, and density structure.

Tab. 1 lists the data sources used in this study following the terminology of Gawarkiewicz and Plueddemann (2020). Technical details about instrumentation and array composition are provided in their paper. All data are mapped onto an hourly grid, either via averaging (rows 1+3-5) or linear interpolation (row 2). Potential ocean water density (referenced to $p = 0$) is calculated using TEOS-10 (McDougall & Barker, 2011). Hydrography measurements on the shelf are taken at different depths along the 95 m isobath: Surface, 7 m, continuously between $\sim 30-70$ m, and 2 m above the bottom. Local wind and atmospheric data are collected by the CP Array's three surface buoys, 3 m above sea level. Surface windstress was computed from wind speed and air density estimates; occasional data gaps in the Inshore Surface Mooring data were replaced with data from the Central and Offshore Moorings, respectively. This replacement is justified since the maximum horizontal distance between the surface buoys (less than 50 km) is much smaller than the atmospheric synoptic length scale, correlations between surface mooring data are large ($> 95\%$), lag-correlations peak at zero-lag, and the residual distribution peak is smaller than the noise.

Table 1. *Data Sources of OOI Coastal Pioneer Array[a] time series analyzed in this study.*

#	Variables	Mooring	Platform	Platform depth	Ocean depth
1	T, S	Inshore Surface M. (ISSM)	Surface Buoy	2 m	95 m
2	T, S, P, ρ	Upstr. Inshore Prof. M. (PMUI)	Profiler	$\sim 30-70$ m	95 m
3	U, V (wind),	Inshore Surface M. (ISSM)			95 m
4	SLP,	Central Surface M. (CNSM)	Surface Buoy	-3 m	135 m
5	T_{air}, RH	Offshore Surface M. (OSSM)			450 m

Note. [a]from Gawarkiewicz and Plueddemann (2020).

Since the instrument configuration does not cover the typical depth range of the seasonal pycnocline (i.e., between 7 and 30 m), mixed-layer depths cannot be estimated. Instead, a bulk estimate of shelf stratification strength σ is defined as the density difference $\Delta\rho$ between the shelf interior and the sea surface using data from the inshore moorings:

$$\sigma|_{\mathrm{shelf}} \equiv \Delta\rho|_{\mathrm{shelf}} = \rho(z = 67\,\mathrm{m})|_{\mathrm{PMUI}} - \rho(z = 0\,\mathrm{m})|_{\mathrm{ISSM}}. \quad (1)$$

Similar shelf stratification estimates have been used by Forsyth et al. (2018) and Lentz et al. (2003). The deepest depth of the Upstream Inshore Profiler Mooring range with consistent data turnout is at $z = 67$ m. According to Linder and Gawarkiewicz (1998)'s climatology of the shelfbreak front, this depth should be mostly undisturbed from both variability of the mixed-layer depth and the frontal foot position, making it an appropriate location for extracting lower layer density estimates so close to the shelfbreak front. The (bulk) stratification estimate exploits data from both inshore moorings that are spatially separated by 9.2 km along the same isobath. Since the shelfbreak bathymetry shows little along-shelf variation across the CP Mooring Array area and the horizontal length scale of atmospheric weather patterns is much larger than this distance, the horizontal misalignment is not expected to affect the results.

2.2 Level 2 Head: Atmospheric Reanalysis Data

Spatial sea level pressure and surface wind data over Northeast America and the adjacent Atlantic is taken from the ERA5 atmospheric reanalysis data set (Hersbach et al., 2018). This study utilizes ERA5 data on a $1°\times1°$-spatial and 6h-temporal grid. When comparing ERA5 data with observations from the CP Array's inshore surface mooring,

zonal surface windstress shows a cross-correlation of $r = 0.95$, zero lag-correlation, and a narrow ($\mathcal{O}(\sigma) = 10^{-2}\,\mathrm{N\ m^{-2}}$) residual distribution with its peak around zero ($\mathcal{O}(\mu) = 10^{-3}\,\mathrm{N\ m^{-2}}$). Thus, ERA5 data seem trustworthy for the purpose of this study.

2.3 Level 2 Head: Connecting surface forcing with subsurface impact

This study aims to identify high-wind events and link them with shelf stratification changes as a metric for the events' ocean mixing impact. The following algorithm takes time series of local wind forcing and the previously defined shelf stratification index as input and outputs a list of individual events and their associated ocean impact. Event forcing and impact are characterized by a set of simple scalar metrics to allow easy comparison between events. Fig. 2 applies the algorithm to an exemplary event while a detailed description is given in the text.

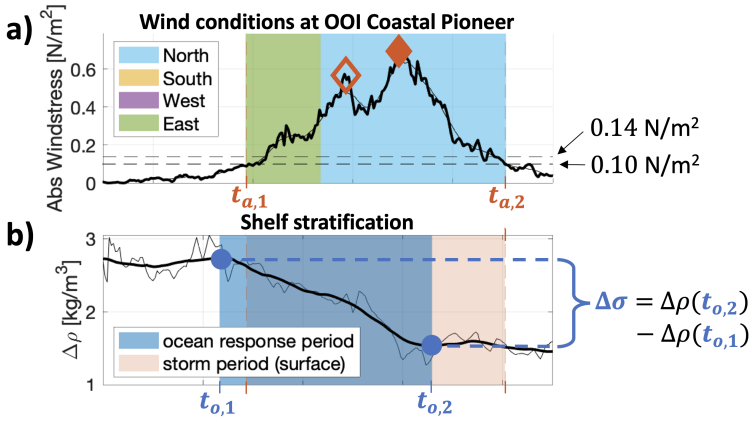

Figure 2. Illustration of how to define a high-wind forcing event, its properties, and subsurface ocean response using local CP Array time series. a) surface windstress (bold line: 1h resolution data; thin line: 12h-moving mean window). b) stratification estimate (bold line: 36h lowpass-filtered; thin line: 1h resolution data). Diamonds and circles are points of interest identified by the algorithm. The algorithm is explained in the text.

Atmospheric high-wind events are defined as peaks above a $0.14\,\mathrm{N\ m^{-2}}$ surface windstress threshold, and both orange diamonds in Fig. 2 represent such peaks. By defining high-wind events as the absence of calm conditions, the beginning and end of an event are determined in a two-step process. First, the smoothed surface windstress (thin black line in Fig. 2a) is examined, and minima are identified on either side of the initial peak below a threshold of $0.10\,\mathrm{N\ m^{-2}}$. Secondly, the beginning and end of an event are found by moving inward from the identified minima until the unsmoothed surface windstress hits the $0.10\,\mathrm{N\ m^{-2}}$ threshold. The two-step process, including smoothing, ensures that cyclones whose relatively calm center passes across the CP Array do not get split into two events. If more than one event peak is associated with the same event time period, the event gets linked with the more prominent peak (see empty vs. filled orange diamond in Fig. 2a).

Defining the beginning and end of a high-wind event allows for integration of atmospheric forcing variables across the event duration, leading to simplified scalar forcing estimates. This study focuses on the integrated along-shelf windstress $\int_{t_{a,1}}^{t_{a,2}} \tau_x \,\mathrm{d}t$ and the cumulative cubed wind speed $\int_{t_{a,1}}^{t_{a,2}} |U|^3 \,\mathrm{d}t$. Since the x-direction aligns well with the shelf edge at the location of the CP Array, no coordinate system rotation is required. The choice of these forcing metrics will be justified in section 6.4. The threshold of $0.14\,\mathrm{N\ m^{-2}}$

represents the upper end of wind force 5 on the Beaufort scale (a little less than 20 knots winds). The comparatively low threshold ensures that the full bandwidth of impact variability associated with wind events is captured. Since Forsyth et al. (2018) apply the same threshold, direct comparison becomes possible. While the chosen threshold affects the number and duration of identified events, the overall results of this study are robust under reasonable threshold parameter variations.

While an event's windstress peak identifies high-wind event forcing, its leading-order ocean response is the net change between the pre- and post-event ocean state, i.e., a derivative variable. The impact of a high-wind event on ocean mixing is quantified by the change in shelf stratification as measured throughout the event. However, since the ocean response may not exactly align with the timing of the locally observed atmospheric forcing, the ocean response time window needs to be determined independently. Fig. 2 illustrates the methodology. An ocean response signal is defined as the stratification estimate difference between two neighboring points of zero slope $\Delta\sigma = \sigma(t_{o,2}) - \sigma(t_{o,1}) = \Delta\rho(t_{o,2}) - \Delta\rho(t_{o,1})$. This simplified approach assumes that the continental shelf is in steady-state ($\partial_t \sigma = 0$) before and after the event and that the high-wind forcing event dominates other potential forcing mechanisms that might be present and change the shelf stratification. We acknowledge the limitations of this assumption, in particular in the presence of other processes, e.g., other high-wind events in the direct vicinity or shelf-break frontal instability. However, the large number of observed events allows us to identify potential outliers where forcing processes could have interacted with one another. Before identifying zero-slope points, the stratification signal is lowpass-filtered ($\mathcal{O}(36\,\mathrm{h})$) to suppress variability from tidal frequencies, daily cycle harmonics, and internal waves. This step ensures that irreversible stratification changes are detected on the time scales associated with synoptic weather events, rather than oscillations occurring at shorter time scales.

Ocean mixing and high-wind forcing events are identified independently before being matched with each other if they overlap in time. If multiple ocean mixing events overlap with a single high-wind event, the wind event is ultimately associated with the larger absolute stratification difference. The exact start and end points of the ocean response event have only a weak dependence on the simplified scalar metric of shelf stratification change, particularly since the data is lowpass-filtered. The algorithm provides a robust approach to identifying locally observed high-wind forcing events, defining their start and end, and linking the forcing with its subsurface ocean mixing impact on the outer continental shelf.

3 Level 1 Head: Seasonal Breakdown of Shelf Stratification

The algorithm described above has been applied to the time series recorded by the CP Array between May 2015 and 2022 (see fall destratification season 2016 in Fig. 3a+b). The fall destratification season is defined as the time period of consistent water column homogenization (Fig. 3c): The start date is set as August 15. The season's end is the time at which the lowpass-filtered stratification signal decreases below the rest stratification threshold $\Delta\rho < 1.0\,\mathrm{kg\ m^{-3}}$ and remains there for the rest of the year. The event that pushes the stratification below the threshold is included in the destratification season. The $1.0\,\mathrm{kg\ m^{-3}}$-threshold ensures that late season density fluctuations are not included in the analysis. Since smaller thresholds only increase the number of events with little ocean mixing impact, the overall results of this study are robust to a range of thresholds.

The annual cycle of seasonal stratification and shelf homogenization follows the climatology outlined in Linder and Gawarkiewicz (1998) despite noticeable interannual variability (Fig. 3c). Interannual variability is observed in the timing of re- and destratification, the peak stratification during late summer, and the magnitude of the remaining

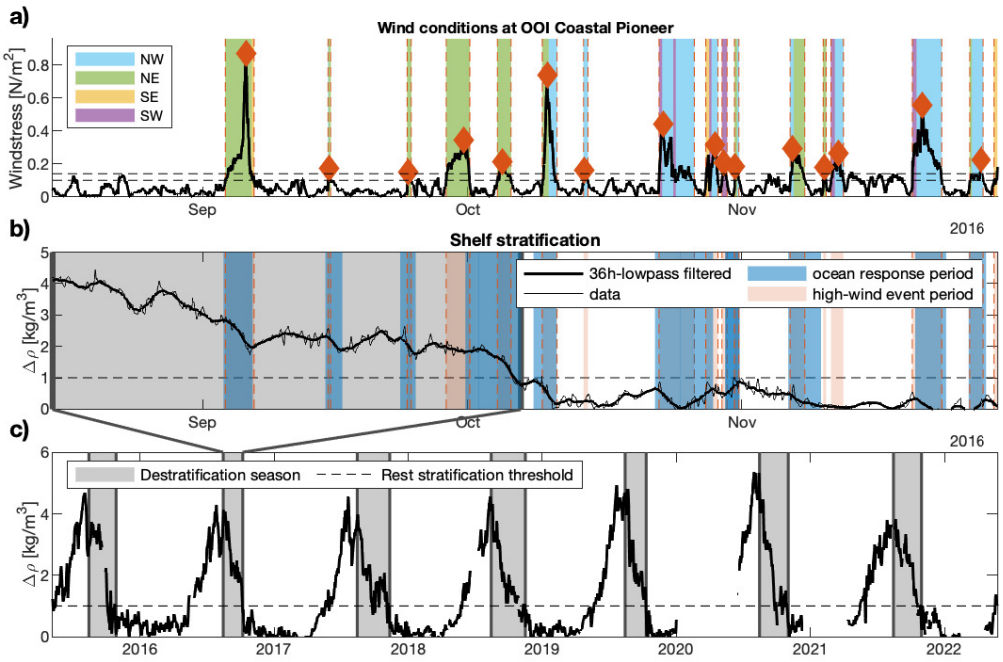

Figure 3. Locally identified high-wind events during fall 2016 and their associated ocean mixing impact by applying the algorithm outlined in section 2.3. a) Surface windstress; main wind directions throughout a high-wind event are color-coded. b) Shelf stratification estimate. Ocean response periods associated with a high-wind event are colored in blue. c) Lowpass-filtered stratification estimate $\Delta\rho$ of full time series (May 2015-2022); destratification seasons are colored in grey.

stratification and its fluctuations persisting throughout the winter. Stratification reaches maximum values around mid-August before it rapidly decays to leave the shelf on average homogenized on October 28±15 days. Tab. 2 lists core information for each destratification season between 2015 and 2021 (left section) and assesses the contribution of destratifying high-wind events to the annual stratification breakdown (right section). The large interannual variability is depicted in the standard deviations across different years which tend to be on the same order of magnitude as the mean signals.

The net destratification from high-wind events alone $\sum_i \Delta\rho_i$ is typically larger than the initial shelf stratification in late summer (ρ_0) by 35±39% averaged across the seven years. This result supports Lentz et al. (2003) who inferred from just four storm events during fall 1996 that the fall destratification on the continental shelf is primarily caused by high-wind forcing and not the cumulative effects from surface cooling throughout the season. Intermittent restratification between high-wind events allows the cumulative effects from destratifying wind events to exceed the initial stratification and prolong the destratification breakdown. Such restratification during calm conditions can be caused by a variety of processes, e.g., surface heating, frontal relaxation, and mixed-layer turbulence. The cumulative change in shelf stratification during calm conditions has a magnitude of 1.3±1.3 kg m^{-3} per season, i.e., net restratification in every but one year. Restratification associated with high-wind events occurs occasionally; though, high-wind forcing dominantly causes destratification.

The number of high-wind events per destratification season varies widely (see Tab. 2), representing the large variability in the atmospheric forcing on synoptic time scales.

Table 2. *Statistics of fall destratification breakdown on the Southern New England shelf (SNES)*

	Destratification season			Destratifying events		
Year	End	Length	ρ_0	N	$\sum_i^N \Delta\rho_i$	$\overline{\Delta\rho_i}$
2015	Oct 28	74 d	3.7	4	-4.0	-1.0
2016	Oct 07	53 d	4.1	4	-2.8	-0.7
2017	Nov 11	89 d	4.0	12	-7.5	-0.6
2018	Nov 16	93 d	4.3	14	-6.2	-0.5
2019	Oct 11	57 d	4.8	9	-7.6	-0.8
2020	Nov 01	78 d	5.2	10	-7.6	-0.8
2021	Oct 30	76 d	3.8	8	-4.9	-0.6
Mean	Oct 28	74 ± 15 d	$4.3 \pm .5$	9 ± 4	-5.8 ± 2.0	$-0.7 \pm .2$

Note. The columns display the year, last day of the destratification season, season length, maximum stratification after August 15, number of destratifying high-wind events during the season, cumulative impact from events, and average impact per event, respectively. The last row presents the mean and standard deviation across all years. Only events associated with destratification are considered. Stratification has units kg m^{-3}.

As shown in Fig. 3a, high-wind events during early winter shortly follow upon each other while they are more sparse during the summer and early fall with large periods of calm conditions. Hurricanes or their extratropical successors can be particularly impactful if they pass close to the shelf. Since the North-Atlantic hurricane season peaks in early September, these events typically influence the shelf when stratification is still high. The signal-to-variability ratio of ocean impact is larger for individual destratifying events than for the cumulative wind-driven impact across the destratification season. This finding suggests that the timing of the stratification breakdown depends more on the number and distribution of high-wind events across the season than on the forcing characteristics of individual events. While each anomaly in the 7-year long data record contains a story worth telling, this study aims to identify the atmospheric patterns that consistently impact the continental shelf every fall.

4 Level 1 Head: Connecting Local Forcing With Regional Patterns

This work aims to identify the high-wind event patterns with the largest ocean mixing impact and contribution to the fall stratification breakdown on the continental shelf. Each local forcing event is part of a large-scale atmospheric pattern with distinct forcing characteristics on the continental shelf. Thus, zooming out and categorizing spatio-temporal atmospheric patterns allows the partition of the highly variable local forcing when examining the wind-driven ocean mixing impact. The goal is to determine which patterns lead to the greatest destratification on the shelf. While section 2.3 provides a framework to link locally observed wind forcing with its ocean mixing impact, its purely local approach does not have the ability to differentiate between different atmospheric patterns.

4.1 Level 2 Head: Categorization Scheme for High-Wind Events

To link local forcing conditions with atmospheric pattern, a categorization scheme is established that clusters spatial sea level pressure patterns whenever a high-wind event gets detected locally by the CP Array. The scheme is motivated by Foukal et al. (2019)'s approach of investigating the origin of storms that are associated with a downwelling ocean

response on the Alaskan Beaufort Sea continental shelf. Even though the scheme categorizes atmospheric forcing events, it is designed with the oceanographic application of linking the forcing with ocean mixing impacts in mind. Thus, the location of an atmospheric pattern with respect to the SNES is an integral part of the categorization since distance and wind direction largely contribute to the local forcing characteristics.

The high-wind event categorization scheme aims to identify the sea level pressure pattern which is mainly responsible for the locally measured forcing. Pattern clustering, rather than a storm tracking algorithm was used to categorize events since high-wind forcing events on the SNES are caused by a wide variety of types and scales of synoptic weather systems. Conventional storm tracking algorithms are typically trained towards identifying closed-contour cyclone systems (Neu et al., 2013). The pattern clustering relies on human-based decision-making when categorizing high-wind events based on their spatio-temporal characteristics. To minimize human bias, a clear three-step protocol for assigning events to a particular pattern category has been established:

1. Identification: Weather systems with closed-contour sea level pressure (SLP) patterns whose isobars reach the CP Array location concurrent with a locally detected wind event (windstress at least $0.14\,\mathrm{N\ m^{-2}}$ at the CP Array) are identified as potential candidates.
2. Selection: The candidate weather systems are ranked based on the alignment between their geostrophically induced winds and the locally observed winds during the $\pm$24h period surrounding the local windstress maximum of the event. The weather system with the best alignment gets selected as the one primarily responsible for the locally observed forcing. If there is doubt about the best alignment, the system with the stronger SLP anomaly is selected.
3. Assignment: The selected pattern gets assigned to one of the pre-determined categories based on its spatio-temporal characteristics and location with respect to the CP Array. In the rare case that a clear distinction among the categories is not possible, the event remains uncategorized.

Events have been categorized by the same person in a random order to avoid establishing artificial temporal trends.

As typical for unsupervised learning frameworks, the number of categories is not inherent to the dataset and needs to be determined externally. Six categories are sufficient to distinguish between the different locally observed wind forcing patterns while remaining able to unambiguously assign a particular category to an event. While increasing the number of categories would statistically reduce the variability per category, the assignment becomes more ambiguous in reality due to less distinct characteristics of individual categories. While four categories are required to differentiate between the four main wind directions associated with slowly-propagating large-scale patterns, only two categories are required to differentiate between propagating cyclones since storm tracks over New England converge and are mostly oriented in the Northeast direction towards the Icelandic Low (Zielinski & Keim, 2003). Note that there is no separation between tropical and extratropical cyclones. The chosen partitioning of large-scale sea level pressure patterns into the presented four categories is recognizable in the spatial modes and principle component values of an Empirical Orthogonal Function (EOF) analysis (not shown).

4.2 Level 2 Head: Partitioning Weather Systems into Six Spatio-Temporal Categories

Applying the human-centered categorization scheme described above, 98% of all locally observed high-wind events have been assigned to one of six categories. Each category is defined by its distinct sea level pressure (SLP) pattern and named after the lo-

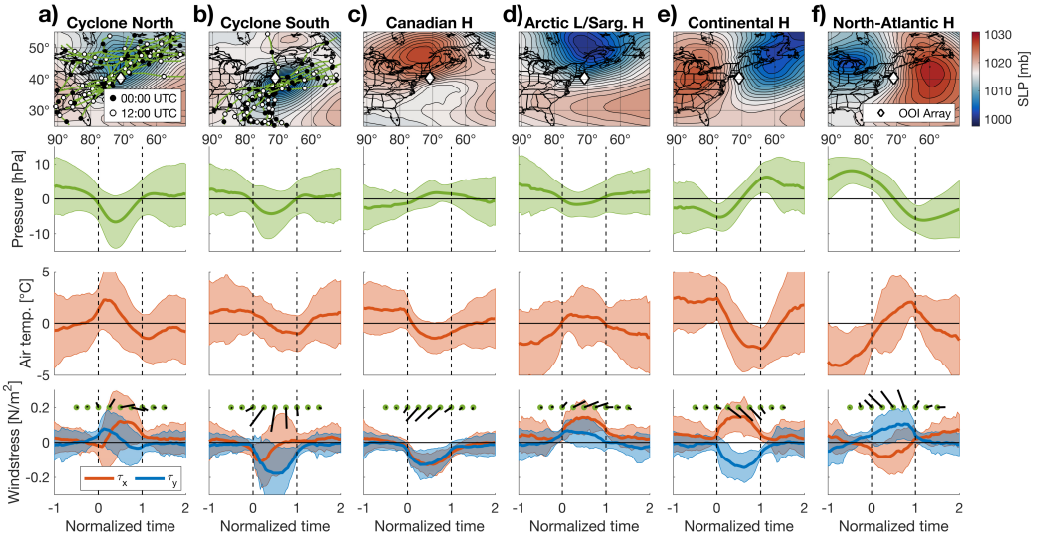

Figure 4. Composites for each high-wind event category (a-f), using categorized high-wind events between May 2015-2022. Row 1: Mean sea level pressure fields at event peaks. Storm tracks (determined manually) are included for all cyclones that occured during the fall destratification seasons. Row 2-4: Time series composites of sea surface pressure (row 2), surface air temperature (row 3), and surface windstress (row 4) from the continental shelf as observed by the CP Array. Time axis is normalized with the event's start at $t = 0$ and end at $t = 1$. For better visualization of the wind field, surface windstress vectors (row 4) are shown in black. Time series envelopes represent one-standard deviation.

cation of their associated SLP core (Fig. 4). In accordance with geostrophic theory, all high-wind event categories are associated with strong SLP gradients at the location of the CP Array at the time of maximum local windstress. The strength of these gradients is either caused by eastward propagating cyclones/storms with diameters of $\mathcal{O}(100\,\mathrm{km})$ (Fig. 4a+b) or typically more steady large-scale patterns of $\mathcal{O}(1000\,\mathrm{km})$ in spatial extent (Fig. 4c-f). Cyclones are separated into two categories based on their storm track with respect to the CP Array and the SNES since the local forcing has opposite wind directions: *Cyclones North* and *Cyclones South*. Large-scale dipole structures of opposite SLP anomaly can lead to sufficiently strong SLP gradients between them for generating high-wind events on the shelf. East-West dipole structures are particularly prominent (Fig. 4e+f) and are named *Continental High* and *North-Atlantic High*. In contrast, large-scale high- and low-pressure systems north and south of the SNES can cause strong gradients on the shelf without another system close-by (Fig. 4c+d). They are called *Arctic Low/Sargasso High* and *Canadian High*, respectively. There are differences in the seasonal occurrence frequencies between the categories as discussed in section 6.1.

While the SLP patterns provide insight into the origin of the locally observed wind forcing on the continental shelf, the composite time series reveal differences between the patterns' temporal forcing development on the SNES. All patterns are associated with strong changes in SLP which indicate the presence of strong geostrophic winds. While the first four categories (Fig. 4a-d) describe forcing due to the passage of a weather system, the two east-west dipole categories (Fig. 4e+f) reveal that wind forcing can peak as well between a high and a low pressure system with an enhanced SLP gradient in between. Abrupt changes in air temperature at an event's beginning or end suggest that the high-wind forcing pattern is associated with a frontal passage.

The spatio-temporal characteristics of each category lead to distinguishable surface windstress patterns on the SNES. The eastward propagation of the comparatively small cyclones leads to rotating winds on the continental shelf, and the spatial relationship between the cyclone and the CP Array determines from where the winds come and how fast they rotate locally. In contrast, large-scale patterns are more stable throughout the event duration and are associated with more steady winds. Frictional drag in the surface boundary layer likely causes the deviation between the SLP isobar orientation at the CP Array location and the windstress vectors towards the low-pressure systems. While Canadian Highs are associated with steady down-front winds, Arctic Lows/Sargasso Highs cause steady up-front winds.

5 Level 1 Head: High-Wind Event Pattern Characteristics

Since the high-wind event categories are associated with different forcing characteristics on the SNES, their average ocean mixing impacts should differ as well. The wind forcing direction is expected to be crucial for predicting ocean mixing impacts on the continental shelf due to the existence of a bathymetric boundary (Gill, 1982). Simple scalar metrics to characterize an event's wind forcing directionality are the mean wind direction $\overline{\phi}$ and its standard deviation[1] σ_ϕ. A small standard deviation represents steady winds throughout the event. Following a two-dimensional Ekman theory argument for the coastal ocean, down-front winds (with the coast to the right on the Northern hemisphere) will likely cause a downwelling-favorable ocean response. The water transport across the surface Ekman layer will be onshore, causing an opposite flow in the interior to conserve mass which results in downwelling at the coastal boundary. Up-front winds will cause the opposite response. Downwelling-favorable (i.e., westward down-front winds) tend to destratify the shelf by advecting denser slope water onshore at the surface and/or steepening the shelfbreak front, potentially leading to frontal instability and additional shelfbreak exchange (Lentz et al., 2003). The onshore Ekman transport

$$V_{Ek} = -\frac{1}{\rho_0 f_0}\tau_x \tag{2}$$

solely depends on the along-shelf surface windstress component τ_x. Since the SNES shelfbreak is nearly aligned with the zonal East-West axis, no coordinate system rotation is required. From Eq. (2), the cumulative (or integrated) zonal surface windstress across an event $\int_{t_{a,1}}^{t_{a,2}} \tau_x \, \mathrm{d}t$ can act as a first-order estimate for the cross-shelf Ekman forcing.

Following the first-order Ekman theory argument outlined above, the cumulative zonal windstress throughout an event is correlated positively with the associated change in stratification (Fig. 5a). The observations replicate the trend observed by Forsyth et al. (2018) in their realistic model study further inshore on the New Jersey shelf (at the 55 m isobath). Downwelling-favorable high-wind events ($\int \tau_x \, \mathrm{d}t < 0$) are associated with destratification ($\Delta\sigma < 0$) and vice versa. The linear trend is statistically different from zero on a 99% confidence interval. For the statistical analysis, events have been treated as independent, which is reasonable since temporal relationships between events are not preserved. Nonetheless, the spread between Ekman forcing and ocean response remains large, particularly for positive cumulative Ekman forcing and when treating all high-wind events alike.

The results from the categorization scheme provide additional information about the individual events, and the categories tend to cluster across the forcing and ocean mixing impact indices. Thus, the categorization allows further distinguishing between distinct forcing patterns and their influence on stratification (Fig. 5). Both, Canadian Highs and Cyclones South cause downwelling-favorable winds on the SNES and are consistently

[1] see Eq. (1) in Yamartino (1984)

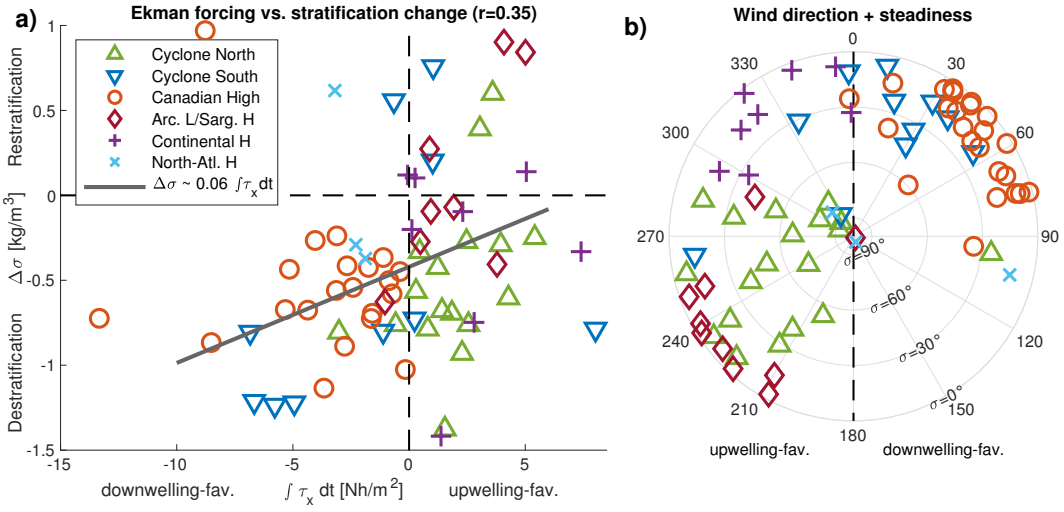

Figure 5. Clustering of high-wind event categories when comparing the local forcing indices with ocean mixing impact for individual events during the fall destratification seasons 2015-2021. a) Cumulative cross-shelf Ekman forcing $\int \tau_x dt$ and stratification change $\Delta\sigma$. The linear trend is a least-squares fit applied to all data shown, while some extreme events are outside the presented axis intervals. b) Leading-order forcing characteristics, including the mean wind direction $\overline{\phi}$ (polar angle of wind origin) and its circular standard deviation σ_ϕ (radial axis); the steadier an event's wind direction, the further it is away from the origin.

associated with destratification. However, their respective clusters differ considerably in their spread. Canadian Highs cluster closely and show comparatively little variability in their forcing magnitude, wind direction, and steadiness. Similar forcing conditions coincide with relatively little spread in their associated ocean mixing impact. Arctic Lows/Sargasso Highs describe opposite local wind conditions since they are associated with fairly steady upwelling-favorable winds. However, these events are not consistently associated with restratification, potentially since local shear-driven destratification can overcome Ekman-driven restratification.

Cyclone clusters show large variability across all characteristics. Since the forcing metrics are purely based on local observations at a defined location, the distance and spatial relationship between a cyclone core ad the CP Array contribute to the magnitudes of the established forcing indices. Cyclones take much less time than large-scale weather systems to pass across distances of the order of their horizontal length scale. In addition, their distance to the CP Array is more variable than for large-scale weather patterns. Combining these spatial properties likely adds to the enhanced variability in the local forcing characteristics and reduces the wind direction steadiness throughout the event. Locally rotating winds throughout the event duration strongly indicate the passage of Cyclones, and the rotation direction depicts whether the Cyclone passes north or south of the CP Array.

Since East-West dipole patterns have stronger wind components in the cross-shelf direction, only considering the along-shelf windstress component likely misses important aspects of the wind forcing. Thus, it is not surprising that East-West dipoles show the strongest deviation from the linear trend between cumulative along-shelf forcing and ocean mixing impact (Fig. 5a).

6 Level 1 Head: Discussion

6.1 Level 2 Head: Intra-seasonal Variability in Event Timing

The high-wind event categorization scheme is solely based on the event characteristics throughout the event, i.e., each event is treated as an independent unit while its placement within the annual cycle and potential interaction with other events are not considered. Since the end of the destratification season fluctuates considerably between years (see Tab. 2), the timing of high-wind events likely affects whether they contribute to the fall stratification breakdown or not. In general, a shift from more downwelling-favorable high-wind events early in the fall to more upwelling-favorable high-wind events later in the fall can be observed in most years (see Fig. 3a for 2016). Grouping the high-wind events by category reveals that this observation is indeed caused by differences in the categories' intra-seasonal timing within the fall season (Fig. 6).

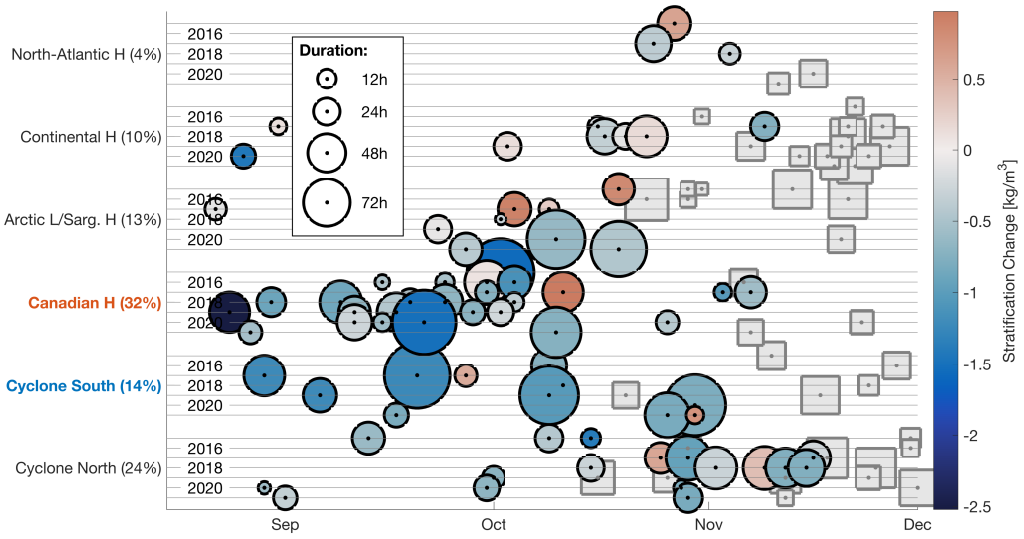

Figure 6. Timing of individual high-wind events within the fall destratification seasons 2015-2021. Events are grouped by category including their frequency of occurrence during the fall destratification (in %). Both, the event duration (marker size) and the associated change in stratification (marker color) are shown. Events that occurred after the stratification breakdown for a given year (see Tab. 2) are shown as grey squares.

Most high-wind event categories cluster on sub-seasonal timescales of roughly 1-2 month length and with sharp edges toward both ends of the distribution. Due to the intermittent nature of high-wind events, seven years of observations are not sufficient to meaningfully determine statistical occurrence distributions. Cyclones South and Canadian Highs tend to occur early in the season, adding to their likelihood to appear in the destratification season. In contrast, East-West dipole patterns and cyclones that propagate further north across New England pick up in late fall/early winter after the stratification breakdown might have already occurred.

Shelf stratification decreases consistently throughout the destratification season, leaving weaker rest stratification for events to affect if they occur late in the season. Thus, the intraseasonal differences in timing between categories might lead to underestimating the ability of individual events late in the destratification season to impact the shelf stratification. However, this work aims to identify the most impactful high-wind weather

patterns for the breakdown of seasonal stratification across the whole destratification season. Both, a high-wind event's timing and forcing are inherent characteristics of each high-wind event category, and both variables contribute to the overall seasonal impact of each category. Thus, disregarding the timing as a characteristic of interest would be unprofitable for the purpose of this work.

6.2 Level 2 Head: Seasonal impact

So far, the characteristics of individual high-wind events and their category assignment have been the focus of the analysis. A category's contribution to the fall stratification breakdown is given by combining ocean impact of individual events and the pattern's occurrence frequency and timing, i.e., $\sum_{i=1}^{N_j} \sigma_{ij} = N_j \cdot \overline{\Delta\sigma_j}$ (total bar height in Fig. 7a). Here, N_j is the number of events per season in the j-th category and $\overline{\Delta\sigma_j}$ the average stratification change per event.

Cyclones South and Canadian Highs are the most important for the fall stratification breakdown on the SNES. Events associated with these categories regularly occur early in the fall season (Fig. 6) and individual events are consistently associated with strong destratification (Fig. 5a). Even though Cyclones South, and in particular hurricanes, might be associated with larger individual destratification signals, the continuous presence of multiple Canadian Highs every year makes this event category the number one contributor to the fall shelf destratification. Events from other high-wind event categories are occasionally associated with equally strong destratification signals (Fig. 5a). However, their intermittency and the variability in their impact results in less dominant contributions to the average seasonal destratification.

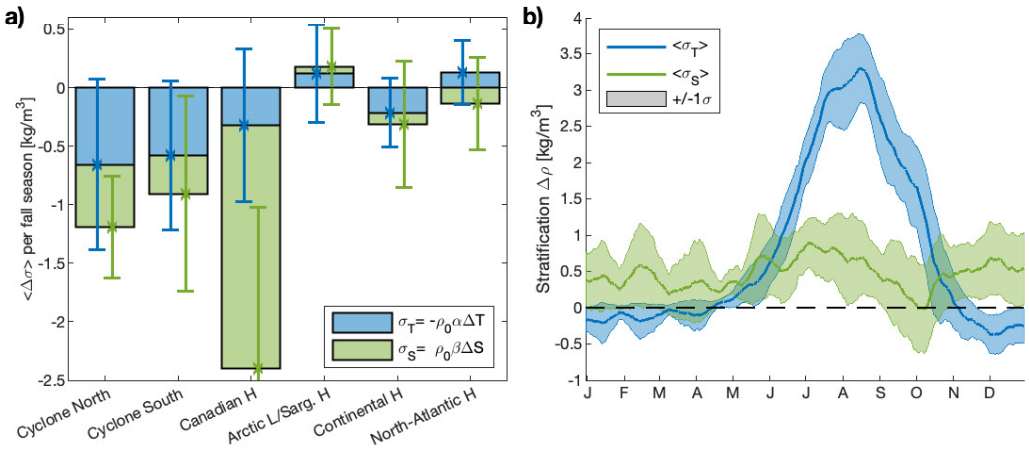

Figure 7. Temperature- (T) and salinity- (S) contributions to stratification on the Southern New England shelf by linearizing the equation of state. a) Cumulative T/S-contributions to the fall stratification breakdown, split by category. b) T/S-contributions to the annual cycle of shelf stratification. The error bars and envelope mark the 1σ-surrounding of interannual variability.

The interannual variability of a category's cumulative contribution to destratification is large due to the strong differences in a category's occurrence between years and the forcing and impact variability of individual events. On a year-to-year basis signals can be hidden. Thus, long multi-year time series are vital for investigating the ocean impact of highly variable atmospheric forcing.

6.3 Level 2 Head: Temperature- and Salinity-Contributions to Stratification Changes

High-wind forcing can lead to mixing and destratification on the continental shelf through a variety of processes, and the forcing characteristics determine the relative importance between such mixing processes. The events associated within each high-wind event category, identified based on their spatial sea level pressure patterns, have similar forcing characteristics on the continental shelf (see Figs. 4+5). Thus, similar mixing processes should be present within a category.

Watermasses can be characterized through temperature (T) and salinity (S), which in turn control density and ultimately stratification via the equation of state (EOS). Thus, distinguishing between T- and S-contributions to the observed stratification changes may allow further insight as to the destratification processes at play. Shelf temperature and salinity can be altered by surface heat- and freshwater-fluxes, respectively, advection, entrainment across the pyncocline, and mixing. By linearizing the EOS and proceeding analogous to Eq. 1, the T- and S-contributions to stratification can be estimated as

$$\begin{aligned} \sigma_T \equiv \Delta\rho_T &= -\rho_0\alpha_T\Delta T = -\rho_0\alpha_T\left[T(z=67\,\mathrm{m}) - T(z=0\,\mathrm{m})\right] \\ \sigma_S \equiv \Delta\rho_S &= \rho_0\beta_S\Delta S = \rho_0\beta_S\left[S(z=67\,\mathrm{m}) - S(z=0\,\mathrm{m})\right] \end{aligned}$$

with the thermal expansion coefficient $\alpha_T(T,S,p) \approx 1.6\times10^{-4}\,\mathrm{K}^{-1}$, the haline contraction coefficient $\beta_S(T,S,p) \approx 7.6\times10^{-4}\,\mathrm{PSU}^{-1}$, and an average reference density $\rho_0 = 1025.8\,\mathrm{kg\ m}^{-3}$. If the shelf heats up, cools, gains salt, and/or freshens non-uniformly across the water column, stratification will change. The net change in T- and S-stratification associated with an individual high-wind event $\Delta\sigma_T$ and $\Delta\sigma_S$ is defined as the difference in stratification throughout the event (analog to section 2.3).

The relative T- and S-contributions to the seasonal destratification differ between different categories with increased interannual variability when distinguishing between T- and S-components instead of focusing on density (Fig. 7). Though, most categories are associated with net destratification on average, seasonal restratification in T and/or S occurs in individual years. Such restratification is less likely for the seasonal T-destratification from Cyclones South and S-destratification from Canadian Highs since the one-sigma error bars do not exceed the multi-year mean signal magnitude.

The initial stratification conditions on the shelf, preceding a high-wind event, likely affect T- and S-contributions to stratification changes. The composition of shelf stratification changes rapidly throughout the destratification season (Fig. 7b). Caused by surface heating during spring and summer, the seasonal stratification is mostly driven by temperature and the seasonal pycnocline typically coincides with the seasonal thermocline (Li et al., 2015). At the end of October, the water column becomes fully temperature-homogenized, and the temperature gradient even reverses with cooler surface temperatures due to surface cooling. Thus, T-destratification becomes less likely for event categories that tend to occur late in the destratification season. In contrast, the S-stratification stays comparatively constant throughout the year since deeper shelf water stays slightly saltier than the surface layer water. However, interannual variability is higher than for temperature, potentially since salinity anomalies are more persistent than temperature anomalies.

Cyclones North, Arctic Lows/Sargasso Highs, and the East-West Dipole patterns cluster later in the destratification season, and S-driven stratification changes are present irrespective of their associated wind directions. In contrast, cyclones that pass south of the continental shelf and Canadian Highs occur early in the season. Nonetheless, they are associated with opposite T/S-signatures of stratification change. The dominance of S-destratification for Canadian Highs exceeds that of any other category. Since timing differences between the two categories are small, differences in the underlying mixing dynamics are likely responsible for the difference.

6.4 Level 2 Head: Attribution to dynamical processes

Opposite temperature- (T) and salinity- (S) contributions to stratification changes may act as fingerprints of different destratification processes. Since high-wind forcing characteristics initiate the dynamical ocean response, the observed T/S-fingerprints in the ocean impact should coincide with differences in the forcing across categories. Both Cyclones South and Canadian Highs are associated with downwelling-favorable winds. Nonetheless, S-destratification is much more dominant for Canadian Highs.

In a horizontally isotropic ocean, the impact of surface forcing on stratification has been modeled by one-dimensional (1D) mixed-layer theory. Surface windstress causes shear in the surface boundary layer, leading to instability, mixing, and entrainment of interior water into the mixed-layer (Price et al., 1986). As a result, the seasonal pycnocline deepens and weakens. As long as ocean currents are negligibly small compared to the high-wind forcing, impacts are identical irrespective of a category's wind direction. The production of turbulent kinetic energy (TKE) from windstress shear $P = -\overline{u'w'}\frac{\partial U}{\partial z} \approx \rho_0^{-1}\tau_x \cdot \frac{\partial U}{\partial z}$ with the horizontal $u = U + u'$ and vertical $w = W + w'$ wind velocity (mean and fluctuation, respectively) is to first-order proportional to $P \sim |U|^3$ (Niiler & Kraus, 1977). The integrated $|U|^3$ throughout a high-wind event represents a simplified estimate for the one-dimensional (1D) mixing potential. Assuming an Osborn-relationship between the eddy diffusivity K_v and the dissipation ϵ (Osborn, 1980) and neglecting buoyancy and transport terms in the TKE-budget, i.e., $P = \epsilon$, the vertical eddy diffusion term from shear-induced mixing scales as well with $|U|^3$:

$$\mathcal{O}\left(K_v \frac{\partial^2 \rho}{\partial z^2}\right) = \mathcal{O}\left(\Gamma \frac{\epsilon}{N^2} \cdot \frac{\partial^2 \rho}{\partial z^2}\right) \overset{P \approx \epsilon}{\underset{\approx}{\downarrow}} \Gamma \cdot \frac{\overbrace{\rho_0^{-1}\tau_x \cdot \frac{|U|}{H}}^{\mathcal{O}(P)}}{\underbrace{\frac{g}{\rho_0}\frac{\Delta\rho}{H}}_{\mathcal{O}(N^2)}} \cdot \frac{\Delta\rho}{H^2} = \frac{\Gamma C_D \rho_a}{gH^2} \cdot |U|^3 \qquad (3)$$

with the mixing efficiency Γ, the drag coefficient of wind C_D, air density ρ_a, and vertical length scale H of the pycnocline width and mixed-layer depth ($\sim 20\,\mathrm{m}$). In the last step, a bulk formula for the surface windstress $\tau_x = \rho_a C_D U^2$ was applied.

The SNES coastline and shelfbreak challenge the 1D mixed-layer theory's isotropy assumption. Two-dimensional (2D) Ekman theory applied to the coastal ocean is consistent with observations of de- and restratification based on the wind directionality as shown in section 5. The cross-shelf Ekman transport is proportional to the along-shelf surface windstress τ_x and given in Eq. (2). Thus, $|U|^3$ and τ_x are two wind forcing variables that are representative of two different ocean response mechanisms: 1D mixing from shear and 2D advection across the shelfbreak, respectively.

While Cyclones South and Canadian Highs are both associated with downwelling-favorable mean winds, differences in their wind direction steadiness and typical wind speeds lead to deviations between the wind forcing estimates associated with 1D- and 2D-driven destratification (Fig. 8). The strongest winds on the SNES are caused by a subset of Cyclones South, leading to the largest 1D mixing potential estimates $\int_{t_{a,1}}^{t_{a,2}} |U|^3 \,\mathrm{d}t$ from local shear production. However, since the cyclones cause comparatively unsteady rotating winds on the SNES, their cross-shelf Ekman forcing estimate $\int_{t_{a,1}}^{t_{a,2}} \tau_x \,\mathrm{d}t$ does not exceed that of the Canadian Highs despite their elevated local wind forcing. In contrast, the Canadian Highs show little variability in their wind direction (Fig. 5b), thus they tend to line up with the branch representing steady downwelling-favorable zonal wind forcing. Destratification magnitudes of strong Cyclones South and Canadian Highs are similar.

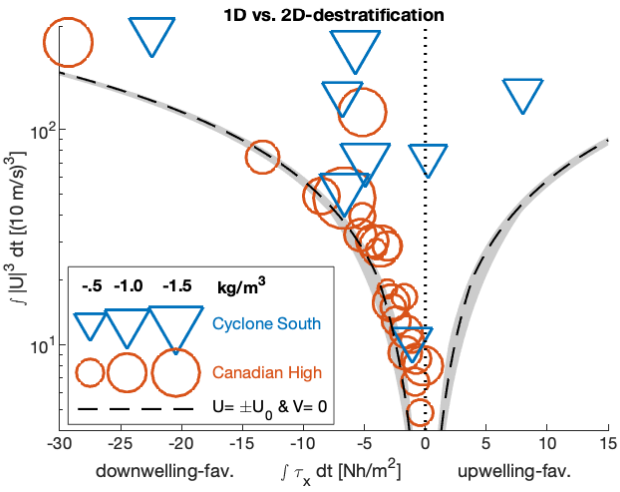

Figure 8. Clustering of Cyclones South and Canadian Highs based on their wind forcing. Y-axis: 1D mixing potential $\int_{a,1}^{a,2} |U|^3 \mathrm{d}t$. X-axis: Cross-frontal Ekman forcing, i.e., cumulative zonal surface windstress $\int_{a,1}^{a,2} \tau_x \mathrm{d}t$. A fully zonal and steady wind event of average duration would lead to values on the two dashed branches while the grey shading covers the 1-sigma envelope of the distribution of high-wind event duration. Marker size depicts the associated destratification strength.

Relating the wind forcing estimates associated with 1D- and 2D-driven destratification to the shelf/slope hydrography, it can be argued that the two estimates should be associated with opposite T/S-fingerprints in the stratification changes from high-wind events. While isotropic mixed-layer theory describes how the 1D mixing potential from shear production is associated with enhanced surface cooling and entrainment of interior cold pool water into the summer-heated mixed-layer, the 2D Ekman forcing causes advection across the shelfbreak. Thus, downwelling-favorable wind forcing causes a surface-intensified onshore advection of salty slope water onto the shelf while cross-shelf temperature gradients throughout the summer mixed-layer are relatively weak. In an idealized setting, each forcing process should lead to a different temperature- and salinity-fingerprint in wind-driven destratification.

Applying the T/S-fingerprint concept to the observational record, the spatial clustering of Cyclones South and Canadian Highs in wind forcing space (Fig. 8) aligns well with the differences in T/S-contributions to stratification changes (Fig. 7): The 1D mixing potential magnitudes are the strongest for Cyclones South that are associated with T-driven destratification while 2D Ekman advection is expected to lead to S-driven destratification. Canadian Highs show such a forcing and ocean response behavior. Further analysis of the velocity fields and cross-shelf gradients would be required to allow a direct comparison between contributions from the two forcing processes in a 2D cross-shelf framework. Unresolved 3D processes from along-shelf gradients and frontal oscillations/instabilities continue to add to the variability.

6.5 Level 2 Head: Frontal Pre-Conditioning

Fingerprints of different forcing processes in the shelf stratification signal have been motivated theoretically and rely on spatial gradients. For example, the simple 2D Ekman-argument to explain the shelf stratification's sensitivity to steady downwelling-favorable winds, and the influx of high-salinity offshore water relies on cross-frontal density gra-

dients across the shelfbreak. The shelfbreak front south of New England consistently separates cooler and fresher continental shelf water from warmer and saltier Slope Sea water, leading to the strongest horizontal density gradients in the region. However, these gradients have not yet been considered despite the CP Array's proximity to the front. In the climatological mean, the frontal jet core is at the 200 m-isobath (Linder & Gawarkiewicz, 1998), while the CP Array's inshore moorings measure around the 95 m-isobath. The shelfbreak front is inherently unstable (e.g., Flagg and Beardsley (1978); Gawarkiewicz and Chapman (1991); Lozier et al. (2002)), leading to ubiquitous meandering and frontal eddies on top of an annual cycle of varying frontal strength.

Frontal pre-conditioning describes the hypothesis that the physical state of the shelfbreak front preceding a high-wind forcing event affects the wind-driven shelf mixing and needs to be included to quantitatively assess the contribution of different forcing processes to destratification. Variability in the frontal state likely adds to the spread observed when comparing the wind forcing with an event's impact on stratification (Fig. 5a). The data record reveals that large stratification changes are regularly associated with rapid changes in temperature and salinity across the water column (not shown). Since the magnitudes of typical surface buoyancy forces are insufficient to explain such observations, onshore advection of the shelfbreak front across the mooring position likely cause these anomalies. Various wind-driven cross-frontal exchange processes have been identified (Houghton et al., 1988; Gawarkiewicz et al., 1996; Mahadevan et al., 2010), and the CP Array is well designed to assess frontal pre-conditioning and shelfbreak exchange events in the future.

7 Level 1 Head: Conclusion

Atmospheric high-wind forcing events and their impact on ocean stratification on the Southern New England shelf (SNES) have been investigated to identify which high-wind event patterns contribute most to the rapid breakdown of stratification during the fall. The variability in the timing of the stratification breakdown is large ($\pm$15 days) and likely depends more on the number and distribution of high-wind events across the season than on the individual forcing characteristics.

A high-wind categorization scheme has been developed to group weather events into six categories based on their spatio-temporal sea-level pressure signal and locally observed wind field on the SNES. Mean composites capture the distinct forcing characteristics inherent with each category. Two event categories are particularly impactful for the seasonal stratification breakdown: Cyclones that pass south of the SNES (*Cyclones South*) and high-pressure systems over eastern Canada (*Canadian Highs*) tend to occur during early fall and are associated with downwelling-favorable winds on the SNES. This result is in good accordance with Ekman theory for the coastal ocean (Gill, 1982) and provides an observation-based measure of interannual variability for the first time.

Cyclones are the most ubiquitous high-wind event pattern in the extratropics. However, cyclones noticeably deviate from the idealized Ekman theory case since local wind vectors tend to continuously rotate throughout a cyclone's passage. As a result, their Ekman cross-shelf circulation cell should be less pronounced than for the steady Canadian Highs. The Canadian Highs establish a real-life representation of the idealized downwelling-favorable Ekman-forcing case on the SNES since the wind forcing is relatively steady throughout the event. Thus, while the strong wind speeds associated with Cyclones South have notable impact on local vertical mixing, Canadian Highs produce a similar strong ocean response with weaker, steadier winds. In addition, their ocean response more likely extends the high-wind forcing duration due to enhanced horizontal advection, post-event restratification, and frontal relaxation.

Differences in mixing processes associated with Cyclones and Canadian Highs are suggested by the opposite temperature- (T) and salinity- (S) contributions to the wind-driven shelf destratification. Cyclones South are associated with larger T-destratification, likely due to their intense wind speeds leading to enhanced local mixing, cold pool water entrainment, and turbulent surface cooling. In contrast, Canadian Highs are weaker; however, their secondary Ekman circulation in the cross-shelf direction causes enhanced S-destratification. Frontal pre-conditioning by the nearby shelfbreak front likely adds to the observed variability in wind-driven ocean impact and should be included to quantify the contribution of cross-shelf exchange processes to destratification on the shelf.

The categorization scheme has shifted the focus from solely interpreting local wind forcing on the continental shelf to studying the ocean impacts of realistic spatio-temporal atmospheric weather patterns. Since local conditions are the product of large-scale weather systems potentially affected by climate change, the categorization results are a first step towards exploring how climate change trends may affect the atmospheric ocean-forcing and contribute to the immense environmental pressure on the New England ecosystem (Pinsky et al., 2013). For example, it is well established that enhanced polar jet stream variability leads to more persistent weather patterns in the mid-latitudes (Francis & Vavrus, 2012), and Chen et al. (2014) have established the impacts of jetstream anomalies on the SNES and beyond.

8 Open Research

The results from the high-wind event categorization scheme and storm tracking can be found at[2] `https://tinyurl.com/34aym8z5`, including all high-wind events observed by the OOI Coastal Pioneer Array (05/2019-11/2022), local forcing and ocean response metrics, and the categorization results using spatio-temporal event characteristics. This work heavily relies on bulk meteorological and subsurface observations from the OOI Coastal Pioneer Array to assess local wind-forcing conditions and stratification changes on the SNES. Data is publically available through multiple gateways, e.g., through the Data Explorer ERDDAP server `erddap.dataexplorer.oceanobservatories.org` (NSF Ocean Observatory Initiative, 2022). Registration is required for download. ERA5 hourly data on single levels was downloaded from the Copernicus Climate Change Service (C3S) Climate Data Store (`doi.org/10.24381/cds.adbb2d47`) and been used to gain spatio-temporal information on high-wind event patterns (Hersbach et al., 2018). Registration is required for download. The mean Gulf Stream position was estimated from the the Monthly Climatology maps of Mean Absolute Dynamic Topography (MADT-H) for 1993-2020, a global gridded (1/4°x1/4°) Ssalto/Duacs data product distributed in delayed time by AVISO+. Data is available through multiple gateways upon registration, e.g., through the Thredds data server (AVISO+, 2022). Thermodynamic properties of seawater have been determined by using the Gibbs-SeaWater (GSW) Oceanographic Toolbox (McDougall & Barker, 2011), Version 3.06.12, available via `teos-10.org/software.htm`.

Acknowledgments

We are grateful for financial support from the German Federal Ministry for Economic Affairs and Climate Action's ERP scholarship fund (LL), grants N00014-21-1-2559 and N00014-19-1-2646 from the Office of Naval Research (GG), and the Scripps Chair for Excellence in Oceanography (AL). We thank Paula Fratantoni for enriching discussions during the early phase of the project. Paula Fratantoni and Svenja Ryan provided valuable comments on the manuscript. Observations are provided by the Ocean Obser-

[2] Permanent object identifier/zotero-doi will follow after peer-review and replace the currently provided link.

vatories Initiative (OOI), which is a major facility fully funded by the National Science Foundation under Cooperative Agreement No. 1743430. The results contain modified Copernicus Climate Change Service information, 2022. The Ssalto/Duacs altimeter products were produced and distributed by the Copernicus Marine and Environment Monitoring Service (CMEMS) (`http://www.marine.copernicus.eu`).

References

AVISO+. (2022). Ssalto/Duacs gridded Mean Absolute Dynamic Topography (MADT-H) Monthly Climatology product (1993-2020). *[Dataset] Thredds Data Server*. Retrieved 2022-12-23, from `tds.aviso.altimetry.fr/thredds/catalog/dataset-duacs-climatology-global/delayed-time/monthly_clim/madt_h/catalog.html`

Beardsley, R., Boicourt, W., & Hansen, D. (1976). Middle Atlantic continental shelf and New York Bight. In M. Cross (Ed.), *Special symposia* (Vol. 2, p. 20-34). American Society of Limnology and Oceanography.

Bengtsson, L., Hodges, K. I., & Roeckner, E. (2006). Storm Tracks and Climate Change. *Journal of Climate*, *19*(15), 3518 - 3543. doi: 10.1175/JCLI3815.1

Chen, K., Gawarkiewicz, G., Lentz, S. J., & Bane, J. M. (2014). Diagnosing the warming of the Northeastern U.S. Coastal Ocean in 2012: A linkage between the atmospheric jet stream variability and ocean response. *Journal of Geophysical Research: Oceans*, *119*(1), 218-227. doi: 10.1002/2013JC009393

Flagg, C. N., & Beardsley, R. C. (1978). On the stability of the shelf water/slope water front south of New England. *Journal of Geophysical Research: Oceans*, *83*(C9), 4623-4631. doi: 10.1029/JC083iC09p04623

Forsyth, J., Gawarkiewicz, G., Andres, M., & Chen, K. (2018). The Interannual Variability of the Breakdown of Fall Stratification on the New Jersey Shelf. *Journal of Geophysical Research: Oceans*, *123*(9), 6503-6520. doi: 10.1029/2018JC014049

Foukal, N. P., Pickart, R. S., Moore, G. W. K., & Lin, P. (2019). Shelfbreak downwelling in the Alaskan Beaufort Sea. *Journal of Geophysical Research: Oceans*, *124*(10). doi: 10.1029/2019JC015520

Francis, J. A., & Vavrus, S. J. (2012). Evidence linking Arctic amplification to extreme weather in mid-latitudes. *Geophysical Research Letters*, *39*(6), L06801. doi: 10.1029/2012GL051000

Francis, J. A., & Vavrus, S. J. (2015). Evidence for a wavier jet stream in response to rapid Arctic warming. *Environmental Research Letters*, *10*(1), 014005. doi: 10.1088/1748-9326/10/1/014005

Gawarkiewicz, G., & Chapman, D. C. (1991). Formation and Maintenance of Shelfbreak Fronts in an Unstratified Flow. *Journal of Physical Oceanography*, *21*(8), 1225 - 1239. doi: 10.1175/1520-0485(1991)021⟨1225:FAMOSF⟩2.0.CO;2

Gawarkiewicz, G., Linder, C. A., Lynch, J. F., Newhall, A. E., & Bisagni, J. J. (1996). A surface-trapped intrusion of slope water onto the continental shelf in the Mid-Atlantic Bight. *Geophysical Research Letters*, *23*(25), 3763-3766. doi: 10.1029/96GL03427

Gawarkiewicz, G., & Plueddemann, A. (2020). Scientific rationale and conceptual design of a process-oriented shelfbreak observatory: the OOI Pioneer Array. *Journal of Operational Oceanography*, *13*(1), 19-36. doi: 10.1080/1755876X.2019.1679609

Gill, A. (1982). Atmosphere-Ocean Dynamics. In *International geophysics series* (Vol. 30). Academic Press.

Hersbach, H., Bell, B., Berrisford, P., Biavati, G., Horányi, A., Muñoz Sabater, J., ... Thépaut, J.-N. (2018). ERA5 hourly data on single levels from 1959 to present. *Copernicus Climate Change Service (C3S) Climate Data Store (CDS)*.

763 doi: 10.24381/cds.adbb2d47
764 Houghton, R., Aikman, F., & Ou, H. (1988). Shelf-slope frontal structure and cross-
765 shelf exchange at the New England shelf-break. *Continental Shelf Research*,
766 *8*(5), 687 - 710. doi: 10.1016/0278-4343(88)90072-6
767 Lentz, S., Shearman, K., Anderson, S., Plueddemann, A., & Edson, J. (2003). Evo-
768 lution of stratification over the New England shelf during the Coastal Mixing
769 and Optics study, August 1996–June 1997. *Journal of Geophysical Research*,
770 *108(C1)*. doi: 10.1029/2001JC001121
771 Li, Y., Fratantoni, P. S., Chen, C., Hare, J. A., Sun, Y., Beardsley, R. C., & Ji,
772 R. (2015). Spatio-temporal patterns of stratification on the Northwest
773 Atlantic shelf. *Progress in Oceanography*, *134*, 123-137. doi: 10.1016/
774 j.pocean.2015.01.003
775 Linder, C. A., & Gawarkiewicz, G. (1998). A climatology of the shelfbreak front
776 in the Middle Atlantic Bight. *Journal of Geophysical Research*, *103(C9)*,
777 18405–18423. doi: 10.1029/98JC01438
778 Lozier, M. S., Reed, M. S. C., & Gawarkiewicz, G. (2002). Instability of a Shelfbreak
779 Front. *Journal of Physical Oceanography*, *32*(3), 924 - 944. doi: 10.1175/1520
780 -0485(2002)032⟨0924:IOASF⟩2.0.CO;2
781 Mahadevan, A., Tandon, A., & Ferrari, R. (2010). Rapid changes in mixed layer
782 stratification driven by submesoscale instabilities and winds. *Journal of Geo-*
783 *physical Research: Oceans*, *115*(C3). doi: 10.1029/2008JC005203
784 McDougall, T., & Barker, P. (2011). Getting started with TEOS-10 and the Gibbs
785 Seawater (GSW) Oceanographic Toolbox. (SCOR/IAPSO WG 127), 28pp. Re-
786 trieved 2020-05-25, from `https://hadoop.apache.org`
787 Neu, U., Akperov, M. G., Bellenbaum, N., Benestad, R., Blender, R., Caballero, R.,
788 ... Wernli, H. (2013). IMILAST: A Community Effort to Intercompare Extra-
789 tropical Cyclone Detection and Tracking Algorithms. *Bulletin of the American*
790 *Meteorological Society*, *94*(4), 529 - 547. doi: 10.1175/BAMS-D-11-00154.1
791 Niiler, P., & Kraus, E. (1977). One-dimensional models of the upper ocean. In
792 E. B. Kraus (Ed.), *Modelling and prediction of the upper layers of the ocean*
793 (p. 143-172). Pergamon.
794 NSF Ocean Observatory Initiative. (2022). Bulk Meteorology Instrument
795 Package (METBK) and CTD (cp03issm-sbd11-06-metbka000, cp01cnsm-
796 sbd11-06-metbka000, cp01cnsm-sbd12-06-metbka000, cp04ossm-sbd11-06-
797 metbka000, cp03issm-rid27-03-ctdbpc000, cp02pmui-wfp01-03-ctdpfk000)
798 data from Pioneer NES Array from 2015-05-09 to 2022-06-01. *[Dataset]*
799 *Data Explorer ERDDAP*. Retrieved 2022-06-17, from `erddap.dataexplorer`
800 `.oceanobservatories.org`
801 O'Reilly, J., & Zetlin, C. (1998). *Seasonal, Horizontal, and Vertical Distribution of*
802 *Phytoplankton Chlorophyll a in the Northeast U.S. Continental Shelf Ecosys-*
803 *tem* (Tech. Rep.). U.S. Department of Commerce. NOAA Tech. Rep. NMFS
804 139.
805 Osborn, T. R. (1980). Estimates of the Local Rate of Vertical Diffusion from Dissi-
806 pation Measurements. *Journal of Physical Oceanography*, *10*(1), 83 - 89. doi:
807 10.1175/1520-0485(1980)010⟨0083:EOTLRO⟩2.0.CO;2
808 Pinsky, M. L., Worm, B., Fogarty, M. J., Sarmiento, J. L., & Levin, S. A. (2013).
809 Marine taxa track local climate velocities. *Science*, *341*(6151), 1239–1242. doi:
810 10.1126/science.1239352
811 Price, J. F., Weller, R. A., & Pinkel, R. (1986). Diurnal cycling: Observations
812 and models of the upper ocean response to diurnal heating, cooling, and wind
813 mixing. *Journal of Geophysical Research: Oceans*, *91*(C7), 8411-8427. doi:
814 10.1029/JC091iC07p08411
815 Roller, C. D., Qian, J.-H., Agel, L., Barlow, M., & Moron, V. (2016). Winter
816 Weather Regimes in the Northeast United States. *Journal of Climate*, *29*(8),
817 2963 - 2980. doi: 10.1175/JCLI-D-15-0274.1

Schofield, O., Chant, R., Cahill, B., Castelao, R., Gong, D., Kahl, A., ... Glenn, S. (2008). The Decadal View of the Mid-Atlantic Bight from the COOLroom: Is Our Coastal System Changing? *Oceanography*, *21*(4), 108–117. doi: 10.5670/oceanog.2008.08

Yamartino, R. J. (1984). A Comparison of Several "Single-Pass" Estimators of the Standard Deviation of Wind Direction. *Journal of Applied Meteorology and Climatology*, *23*(9), 1362 - 1366. doi: 10.1175/1520-0450(1984)023⟨1362:ACOSPE⟩2.0.CO;2

Zielinski, G. A., & Keim, B. D. (2003). *New England Weather, New England Climate*. University Press of New England.

Figure 1.

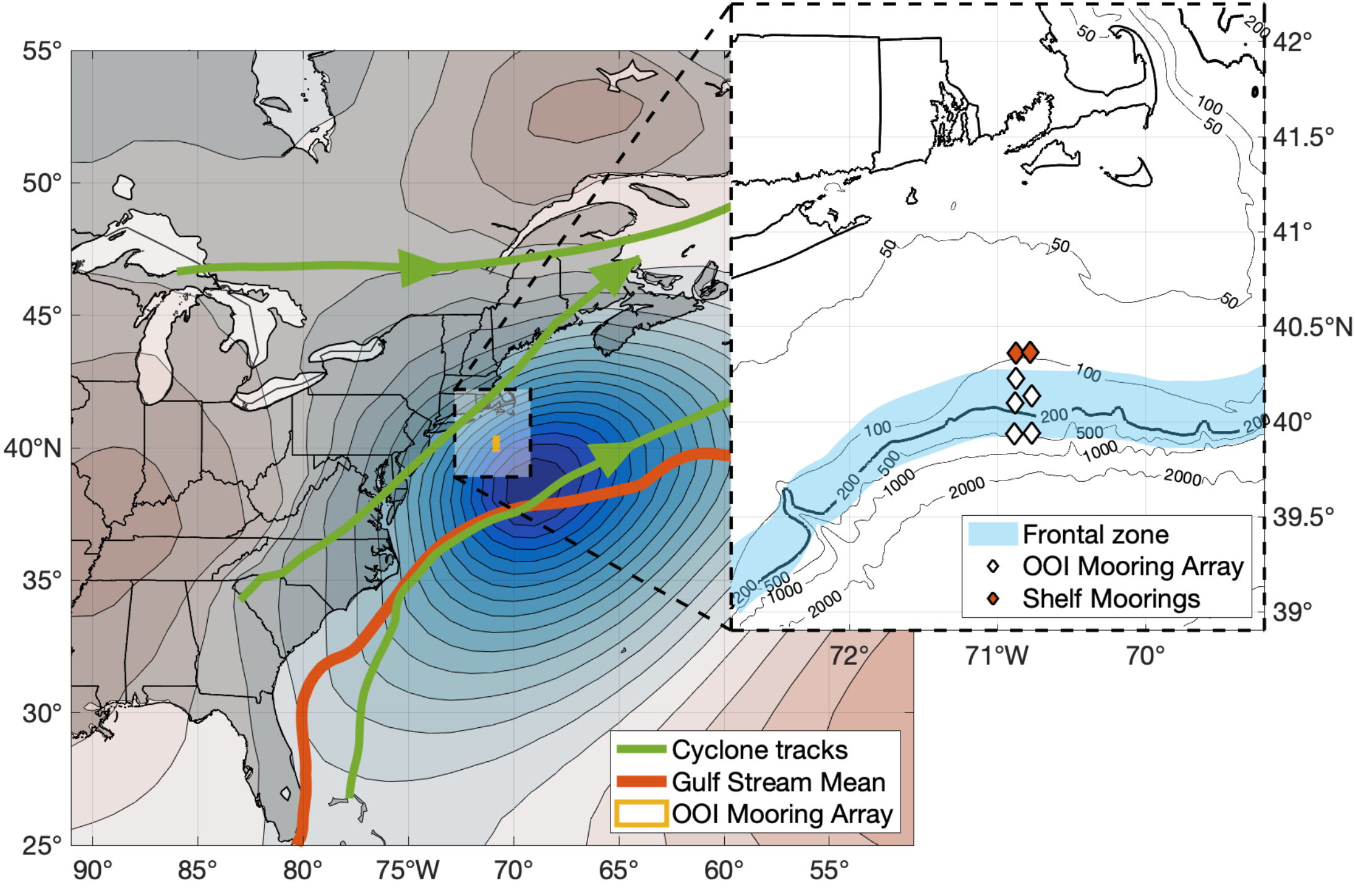
55°
50°
45°
40°N
35°
30°
25°
90°
85°
80°
75°W
70°
65°
60°
55°
72°
Cyclone tracks
Gulf Stream Mean
OOI Mooring Array
42°
41.5°
41°
40.5°N
40°
39.5°
39°
71°W
70°
50
100
200
500
1000
2000
Frontal zone
OOI Mooring Array
Shelf Moorings

Figure 2.

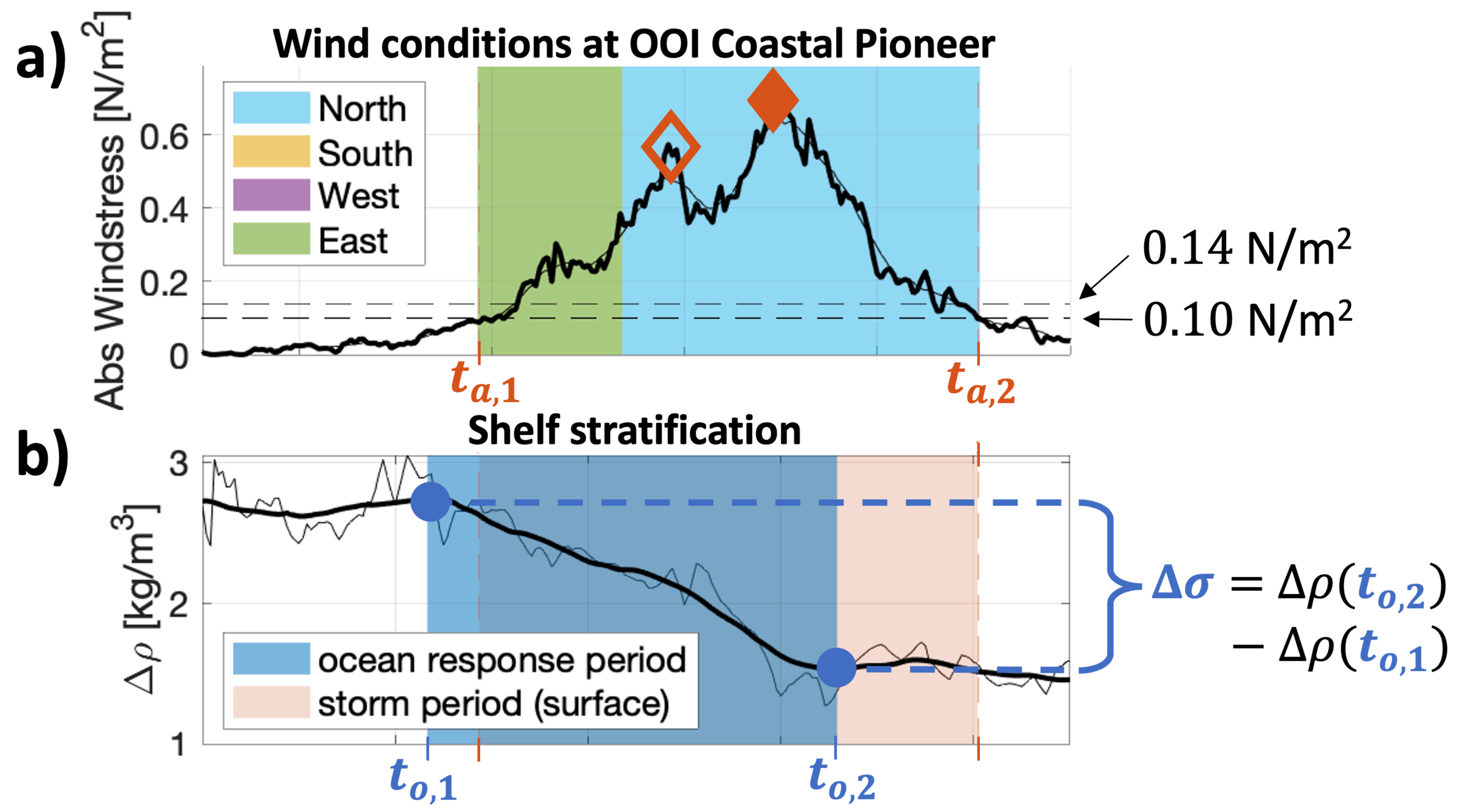
a)
Wind conditions at OOI Coastal Pioneer
Abs Windstress [N/m^2]
0.6
0.4
0.2
0
North
South
West
East
0.14 N/m^2
0.10 N/m^2
$t_{a,1}$
$t_{a,2}$
b)
Shelf stratification
$\Delta\rho$ [kg/m^3]
3
2
1
ocean response period
storm period (surface)
$t_{o,1}$
$t_{o,2}$
$\Delta\sigma = \Delta\rho(t_{o,2}) - \Delta\rho(t_{o,1})$

Figure 3.

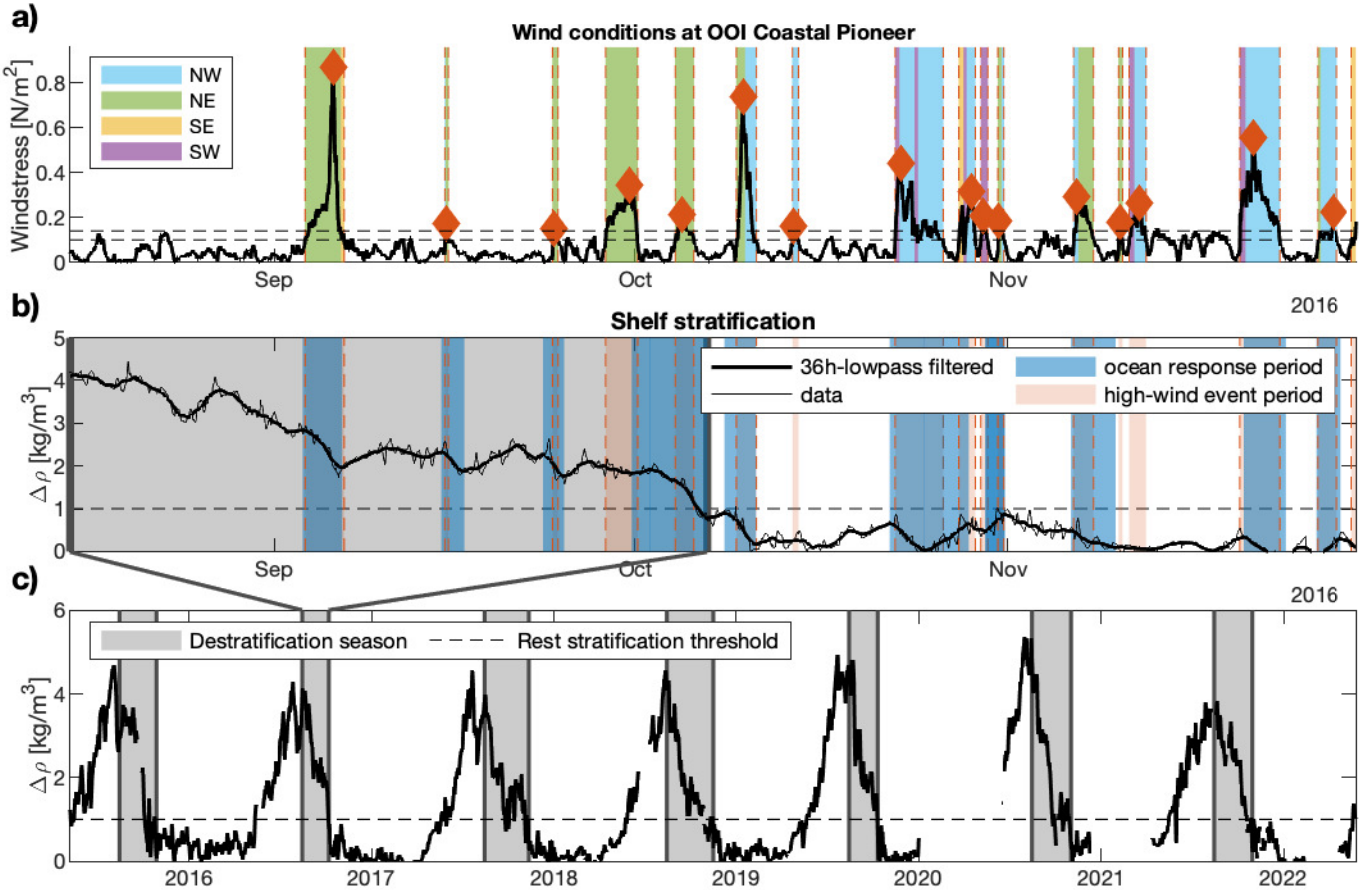
a)
Wind conditions at OOI Coastal Pioneer
Windstress [N/m^2]
NW
NE
SE
SW
Sep
Oct
Nov
2016
b)
Shelf stratification
$\Delta\rho$ [kg/m^3]
36h-lowpass filtered
data
ocean response period
high-wind event period
Sep
Oct
Nov
c)
2016
Destratification season
Rest stratification threshold
$\Delta\rho$ [kg/m^3]
2016
2017
2018
2019
2020
2021
2022

Figure 4.

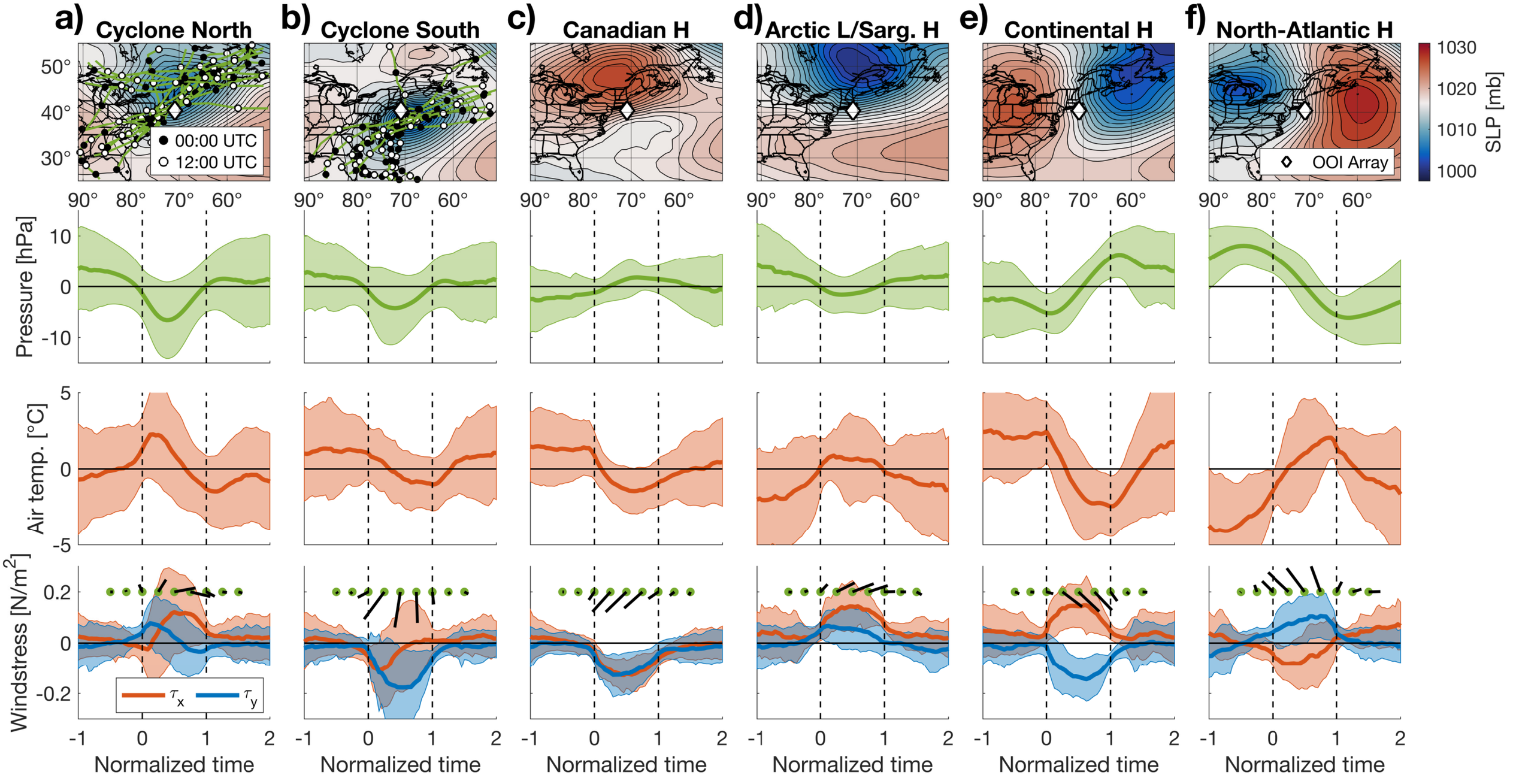
a) Cyclone North
b) Cyclone South
c) Canadian H
d) Arctic L/Sarg. H
e) Continental H
f) North-Atlantic H
00:00 UTC
12:00 UTC
OOI Array
SLP [mb]
1030
1020
1010
1000
50°
40°
30°
90° 80° 70° 60°
Pressure [hPa]
10
0
-10
Air temp. [°C]
5
0
-5
Windstress [N/m^2]
0.2
0
-0.2
τ_x
τ_y
-1 0 1 2
Normalized time

Figure 5.

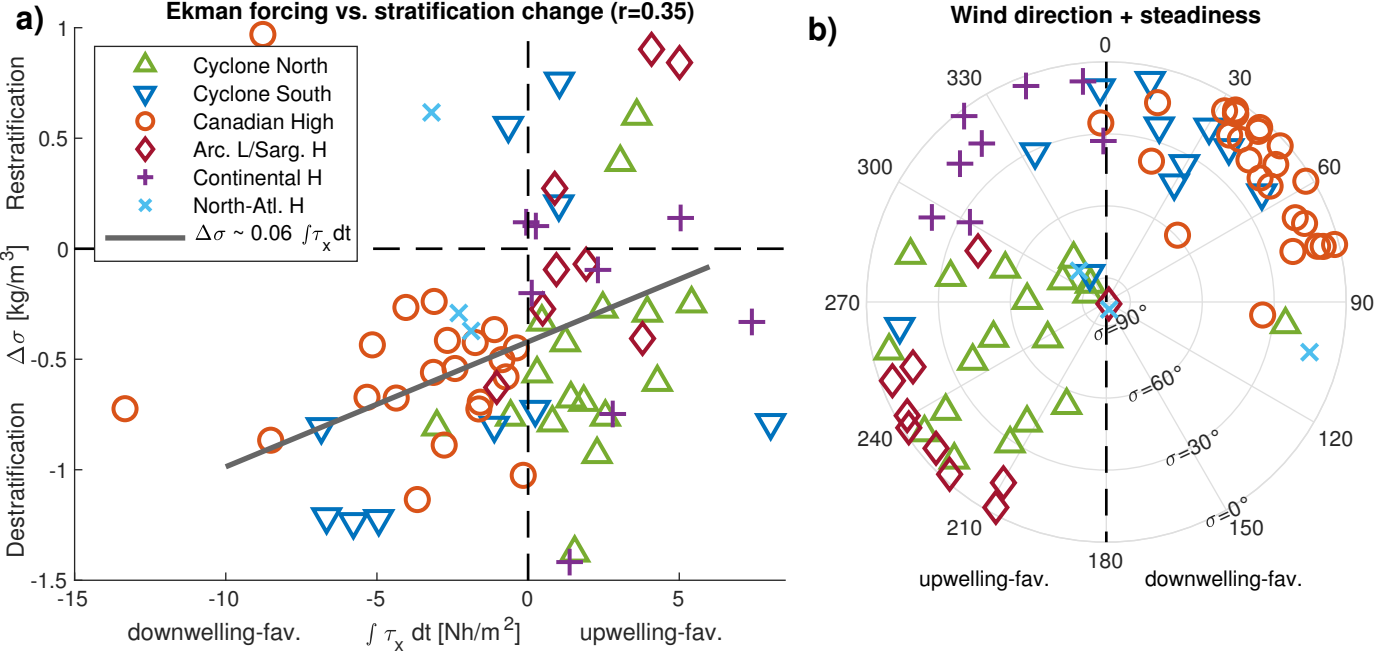
a)
Ekman forcing vs. stratification change (r=0.35)
Cyclone North
Cyclone South
Canadian High
Arc. L/Sarg. H
Continental H
North-Atl. H
Δσ ~ 0.06 ∫τx dt
Restratification
Destratification
Δσ [kg/m3]
1
0.5
0
-0.5
-1
-1.5
-15
-10
-5
0
5
downwelling-fav.
∫ τx dt [Nh/m2]
upwelling-fav.
b)
Wind direction + steadiness
0
30
60
90
120
150
180
210
240
270
300
330
σ=90°
σ=60°
σ=30°
σ=0°
upwelling-fav.
downwelling-fav.

Figure 6.

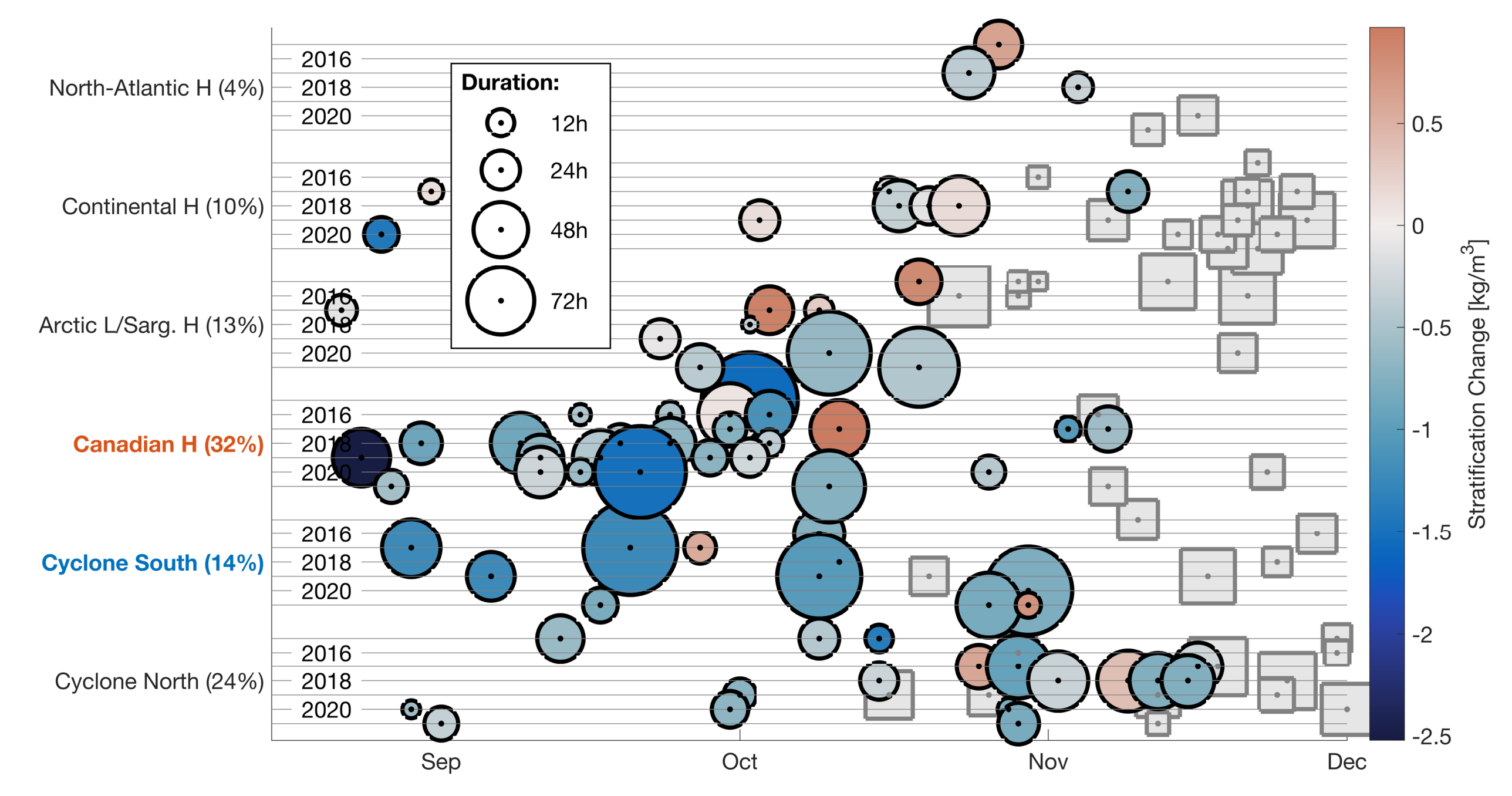
North-Atlantic H (4%)
Continental H (10%)
Arctic L/Sarg. H (13%)
Canadian H (32%)
Cyclone South (14%)
Cyclone North (24%)
2016
2018
2020
Duration:
12h
24h
48h
72h
Sep
Oct
Nov
Dec
0.5
0
-0.5
-1
-1.5
-2
-2.5
Stratification Change [kg/m3]

Figure 7.

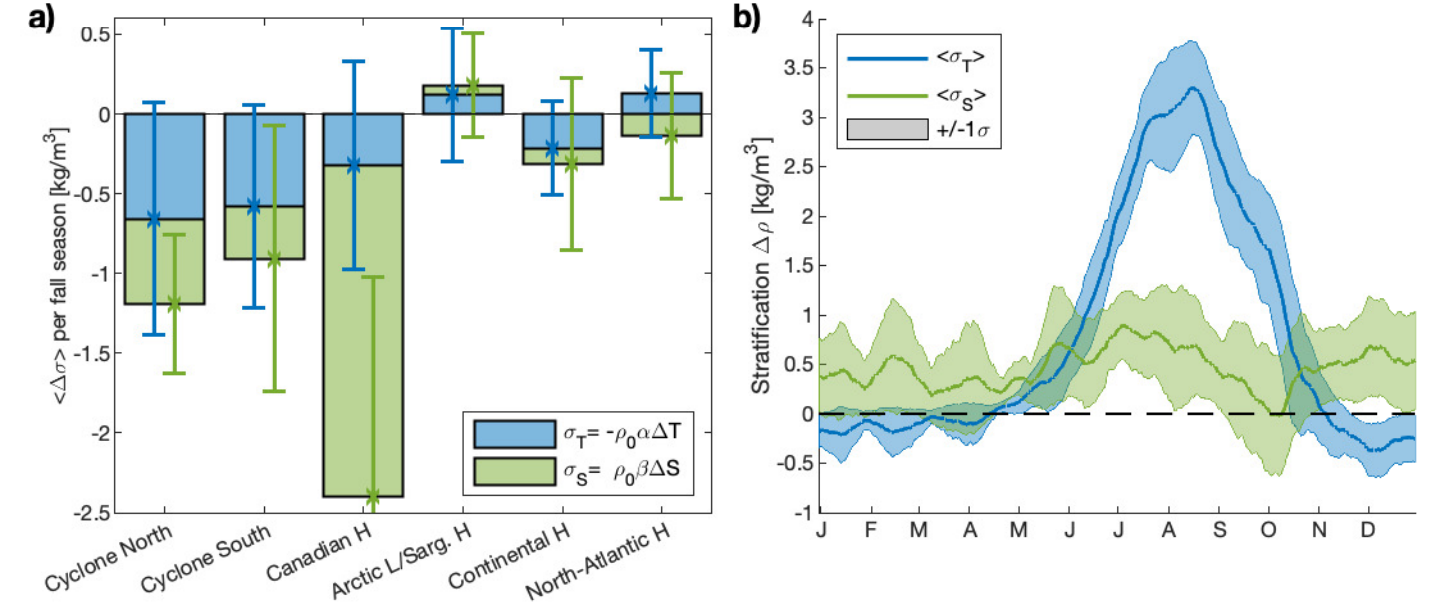
a)
b)
<Δσ> per fall season [kg/m3]
Stratification Δρ [kg/m3]
σT= -ρ0αΔT
σS= ρ0βΔS
<σT>
<σS>
+/-1σ
Cyclone North
Cyclone South
Canadian H
Arctic L/Sarg. H
Continental H
North-Atlantic H
J F M A M J J A S O N D

Figure 8.

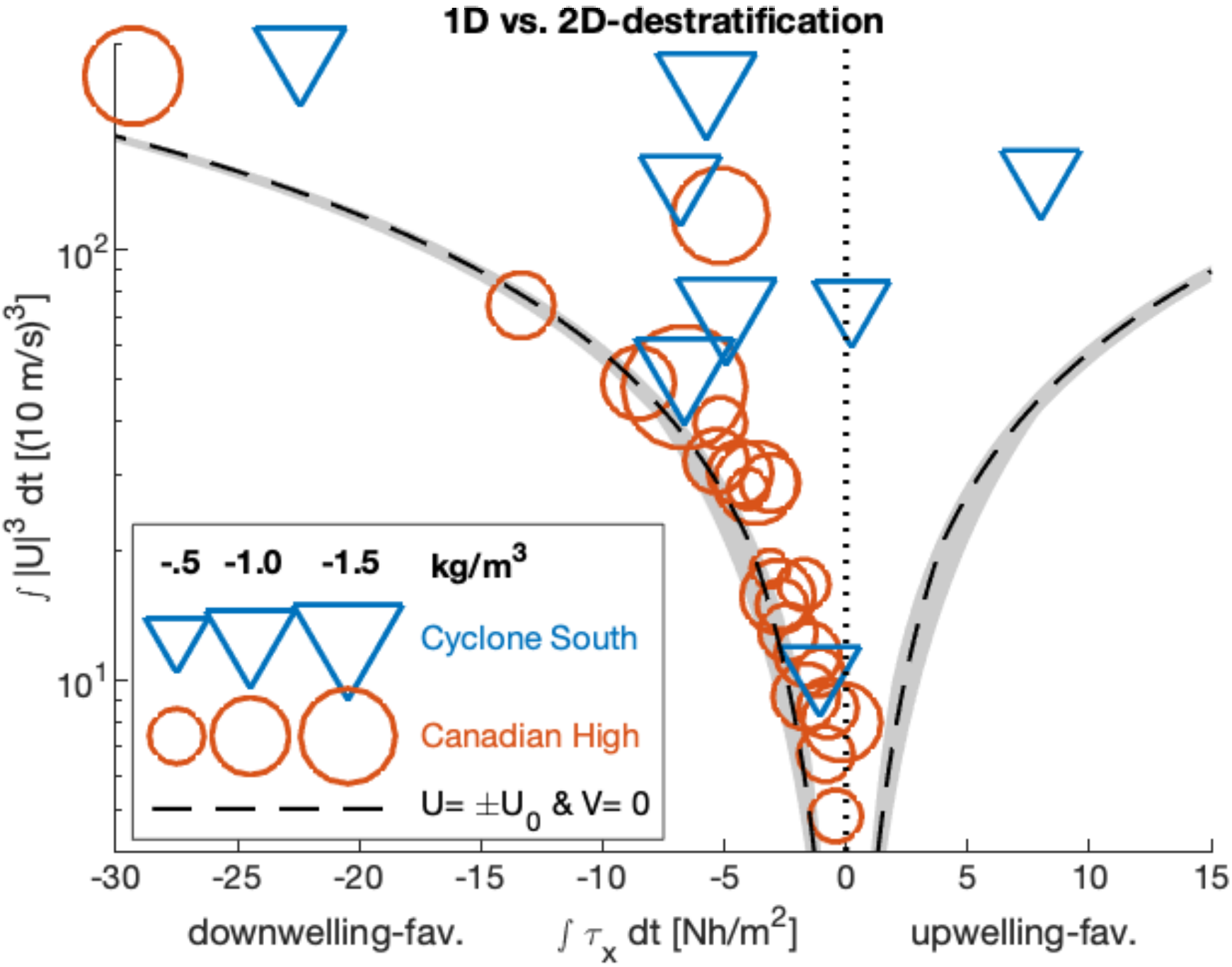
1D vs. 2D-destratification
$\int |U|^3$ dt [(10 m/s)^3]
10^2
10^1
-.5 -1.0 -1.5 kg/m^3
Cyclone South
Canadian High
U= $\pm U_0$ & V= 0
-30 -25 -20 -15 -10 -5 0 5 10 15
downwelling-fav.
$\int \tau_x$ dt [Nh/m^2]
upwelling-fav.